

# Complex Wavenumber Fourier Analysis of the P-Version Finite Element Method

Lonny L. Thompson and Peter M. Pinsky

Department of Civil Engineering, Stanford University  
Stanford, California 94305-4020

---

## Abstract

High-order finite element discretizations of the reduced wave equation have frequency bands where the solutions are harmonic decaying waves. In these so called ‘stopping’ bands, the solutions are not purely propagating (real wavenumbers) but are attenuated (complex wavenumbers). In this paper we extend the standard dispersion analysis technique to include complex wavenumbers. We then use this complex Fourier analysis technique to examine the dispersion and attenuation characteristics of the p-version finite element method. Practical guidelines are reported for phase and amplitude accuracy in terms of the spectral order and the number of elements per wavelength.

---

Computational Mechanics  
Vol.13, pp. 255-275 (1994)

(Communicated by S.N. Atluri, March 30, 1993)

## **1 Introduction**

Computational methods for solving vibration and wave propagation problems introduce errors which distort the physical nature of the computed wave motion. Describing those errors by invoking concepts which originated in mathematical physics, such as dispersion and amplitude attenuation has provided a greater understanding of the numerical methods. In this respect, Fourier analysis has provided an indispensable tool for measuring the accuracy of wave propagation traveling through a finite element spatial discretization of a continuum. Previous researchers in this area have generally restricted themselves to studying the ability of the finite element spatial discretization to admit purely propagating wave solutions. This type of analysis amounts to a discrete Fourier synthesis of the finite element method with pure real wavenumbers. The information obtained from real wavenumber Fourier analysis has been used by Belytschko and Mindle (1980) to study the effect of various mass approximation techniques on the accuracy of Bernoulli-Euler beam elements and by Mindle and Belytschko (1983) to study Timoshenko beam elements. Underwood (1974) used real wavenumber analysis to study axisymmetric shells and rings, while Park and Flaggs (1984,1985) applied this technique to study shear locking and spurious modes found in Reissner/Mindlin plate elements.

To date, most of the effort in the study of the dispersive characteristics of finite element discretization has been limited to low-order elements. The most notable exception is the real wavenumber dispersion analysis of a quadratic bar element by Belytschko and Mullen (1978). In this study, the dispersion analysis revealed the existence of a 'stopping' band in the frequency spectrum of quadratic elements, where solutions in this frequency range decay exponentially. The ramifications of these stopping bands in the context of finite element analysis were not fully understood, although there is some discussion in Belytschko and Mullen (1978) and Abboud and Pinsky (1992).

In this paper, the technique of complex wavenumber Fourier analysis is used to examine the accuracy of higher order finite element discretizations. This complex wavenumber dispersion analysis allows for all wavenumber solutions satisfying the finite element dispersion relation, either real, imaginary or complex. The complex wavenumber may correspond to either a propagating wave (real wavenumber), evanescent wave (imaginary wavenumber), or a harmonic decaying wave (complex wavenumber). This extension of the usual procedure involves only a slight modification to the standard Fourier analysis yet allows for a complete characterization of the 'stopping' bands found in higher order finite element discretizations. Complex wavenumber Fourier analysis can also be used to investigate other systems where complex wavenumbers are present, such as the subsonic, leaky and evanescent waves present in the finite element dispersion analysis of fluid-loaded plates; see Jasti (1992) and Grosh and Pinsky (1996).

We apply this technique to study the dispersion and attenuation characteristics of

p-version finite element methods up to order  $p=5$ . In recent years, there has been a resurgence of interest in elements of high degree, for example Babuska and Suri (1990) and Maday and Patera (1989). In p-refinement the effects of numerical dispersion can be minimized by increasing the spectral order  $p$  of the finite element interpolation functions, while holding the number of elements constant. In contrast, standard h-refinement is achieved by holding the spectral order fixed while increasing the number of elements. The h- and p-versions are just special applications of the finite element method, which allows changing the mesh concurrently with increasing the spectral order  $p$ ; this general approach is called the hp-version. The complex Fourier analysis will characterize the accuracy in terms of both  $h$  and  $p$  refinements over the entire range of complex wavenumbers. Three different p-extensions are considered: (a) Hierarchic Legendre basis functions, (b) Hierarchic Fourier basis functions, and (c) Lagrange interpolations in conjunction with Lobatto quadrature.

Results from the dispersion analysis provides a guide for adaptive solution schemes in the form of an *a priori* error estimate. For example, the dispersion error determined from the analysis of high-order p-version methods could be used as a measure for selecting the required spectral order and mesh size at a given frequency in an adaptive solution. The work of Friberg and Moller (1987) is an example of an adaptive procedure for vibration problems using hierarchic elements. Results from the analysis can also be used to design efficient high order preconditioners for iterative solution techniques as in Babuska, Craig, Mandel, and Pitkaranta (1991) and Barragy and Carey (1991). Deville and Mund (1992) used the concept of complex wavenumbers to determine the spectral radi of various discretizations in studying finite element preconditioned collocation schemes.

In addition, Fourier analysis can be used as a tool to design modifications to the standard finite element method that minimize or eliminate numerical dispersion over a wide range of frequencies. Alvin and Park (1991) used discrete Fourier analysis to assist in the design of tailored mass and stiffness matrices such that the discrete characteristic dispersion curves approximate, for a specified range of frequencies, the continuum case.

The Galerkin/least squares methodology (GLS) is another technique used to improve the dispersion errors found in finite element discretizations. The GLS methodology was originally developed by Hughes, Franca, and Hulbert (1989) to correct the stability problems found in the numerical computation of the advection-diffusion equation. The GLS technique has since been applied by Shakib and Hughes (1991) to the Navier-Stokes and other fluid mechanics problems. Recently, the method has been extended to the reduced wave equation by Harari and Hughes (1991a,1991b). For a Fourier analysis of the GLS method in multi-dimensions see Thompson and Pinsky (1995).

In Section 2 we review the analytic Fourier analysis of a continuous bar. The resulting dispersion curves will serve as a basis for comparison to the discrete dispersion curves obtained from a complex wavenumber Fourier synthesis of p-version

finite element discretizations. In Section 3 we extend standard finite element dispersion analysis to include complex wavenumbers and apply this technique to the discrete complex Fourier analysis of p-type discretizations. Of particular interest from this analysis is the presence of complex wavenumber bands (stopping bands) that occur in these high-order elements and their practical significance. The results of the analysis show that increased phase accuracy is obtained with increasing spectral orders  $p$ . In Section 4 a direct connection is established between the results from our Fourier analysis and the dispersion and eigenvalue results obtained from the p-version finite element solution of an example boundary value problem. Finally we show how information obtained from the Fourier analysis can be used to post-process p-type finite element solutions in order to isolate component waves. By superposition of these wave components, global sinusoidal interpolation can be constructed which better represents the eigenmodes present in the solution.

## 2 Fourier analysis of the continuous problem

The governing differential equation for the steady-state displacement response,  $\phi$  for a uniform elastic bar is the reduced wave equation or so-called Helmholtz equation,

$$\frac{d^2\phi(x)}{dx^2} + \frac{\omega^2}{c^2}\phi(x) = f \quad (1)$$

where  $c = \sqrt{E/\rho}$  is the phase velocity,  $E$  is the Young's modulus,  $\rho$  is the mass density and  $f$  is the forcing function. The assumed time dependence is  $e^{-i\omega t}$  and  $\omega$  is the circular frequency. This equation serves as a model for many other physical phenomena including structural acoustics and electromagnetic wave propagation. The Fourier analysis of the reduced wave equation is accomplished by transforming the problem from the spatial ( $x$ ) domain to the wavenumber domain ( $k$ ) by seeking complex exponential solutions for the displacement of the form,

$$\phi(x) = Ae^{ikx} \quad (2)$$

with constant amplitude  $|\phi| = A$ . We interpret the spatial contribution to the wave solution as the integrand of the Fourier transformation in which the wavenumber  $k$  represents the continuous spatial frequency with wavelength  $2\pi/k$ . The complex Fourier transform is defined as,

$$\tilde{F}(k) := \frac{1}{\sqrt{2\pi}} \int_{-\infty}^{\infty} F(x)e^{ikx} dx \quad (3)$$

Substituting the complex exponential solution (2) into the homogeneous form of (1), or equivalently applying the complex Fourier transform (3), we obtain its characteristic equation in the nondimensional form,

$$(kh)^2 = (\omega h/c)^2 \quad (4)$$

where  $h$  is a problem dependent characteristic length. The properties of the solutions to (4) are: (a) The nondimensional wavenumber ( $kh$ ) is linearly proportional to the nondimensional frequency ( $\omega h/c$ ) over all frequencies, and (b) The wavenumbers occur in pairs  $\pm kh$  of purely real numbers corresponding to propagating free waves in both  $\pm x$  directions. With  $c$  constant, the phase velocity is independent of frequency and the medium is nondispersive.

In contrast to the continuum bar, it is found that finite element solutions have a dispersive character. Many naturally occurring discrete systems exhibit similar dispersive properties. Examples include periodic lattices of polyatomic molecules studied by Brillouin (1953), and periodic composite structures studied by Silva (1991) and others.

### 3 Complex Fourier analysis of p-type elements

In this section we describe a discrete Fourier transform counterpart to the analytical Fourier transform (3). It will be applied to the  $p$ -type discretization of the continuous bar, in order to obtain the characteristic equation relating frequency and wavenumber. Since the wavenumbers obtained through the discrete Fourier transform are in general complex, we are able to obtain real, imaginary or complex wavenumber solutions. The analysis is demonstrated for the one-dimensional reduced wave equation, however results obtained from studying this equation are useful for multi-dimensional discretizations where spatial variations and wave propagation is restricted to one dimension.

The Galerkin method seeks the approximate solution  $\phi^h$  in the complex Hilbert space  $H^1(\Omega)$  such that for all weighting functions  $w^h \in H^1(\Omega)$ ,

$$A(w^h, \phi^h) = L(w^h) \quad (5)$$

The dynamic stiffness operator is,

$$A(w^h, \phi^h) = \int_{\Omega} \left( \frac{d\bar{w}^h}{dx} \frac{d\phi^h}{dx} - \frac{\omega^2}{c^2} \bar{w}^h \phi^h \right) d\Omega \quad (6)$$

with the forcing operator,

$$L(w^h) = \int_{\Omega} \bar{w}^h f d\Omega \quad (7)$$

and the overbar indicates the complex conjugate. For Fourier analysis,  $\Omega = (-\infty, \infty)$ , so that no end-point boundary conditions are considered.

Consider the finite element approximation of the solution,

$$\phi^h(\xi) = \sum_{a=1}^{p+1} N_a(\xi) \phi_a \quad \xi \in [-1, 1] \quad (8)$$

where  $N_a(\xi)$  are shape functions with compact support defined in the local element coordinate  $\xi$ , and  $p$  is the spectral order. Three different finite element approximations to the solution space  $\phi^h \in H^1$  are considered : (1) Hierarchic Legendre shape functions , (2) Hierarchic Fourier shape functions , and (3) Lagrange shape functions with Lobatto quadrature.

For all three interpolations, the frequency dependent dynamic stiffness matrix is defined as the linear combination of stiffness and mass matrices,

$$\mathbf{s}^e = [s_{ab}^e] \in \mathbb{R}^{(p+1) \times (p+1)} \quad (9)$$

$$s_{ab}^e = k_{ab}^e - \omega^2 m_{ab}^e \quad a, b = 1 : p + 1 \quad (10)$$

The stiffness and mass matrices are respectively,

$$k_{ab}^e = \frac{2}{h} \int_{-1}^1 \frac{dN_a}{d\xi} \frac{dN_b}{d\xi} d\xi \quad \text{and} \quad m_{ab}^e = \frac{h}{2c^2} \int_{-1}^1 N_a N_b d\xi \quad (11)$$

where  $h$  is the element length.

### Hierarchic Legendre Basis

Let  $\mathcal{S}^p \subset H^1$  be the finite element subspace of continuous piecewise polynomials of degree  $p$  denoted by  $\mathcal{P}^p$ .

$$\mathcal{S}^p = \{\phi | \phi \in C^0(\Omega), \phi \in \mathcal{P}^p(\Omega_e)\}$$

We start with the standard linear nodal shape functions,

$$N_a(\xi) = \frac{1}{2}(1 + \xi_a \xi) \quad a = 1, 2 \quad (12)$$

and then add to these in a hierarchical fashion internal shape functions defined in terms of integrals of Legendre polynomials.

$$N_a(\xi) := \frac{1}{\|P_{a-2}\|} \int_{-1}^{\xi} P_{a-2}(\xi') d\xi', \quad a = 3, 4, \dots, p + 1 \quad (13)$$

with the norm of the Legendre polynomial,

$$\|P_{a-2}\|^2 = \frac{2}{2a-3} \quad (14)$$

These functions are constructed such that  $N_a(\pm 1) = 0$ . As a result of this property the variables  $\phi_1 = \phi^h(-1)$  and  $\phi_2 = \phi^h(1)$  define discrete nodal variables, while the values  $\phi_a, a \geq 3$  compose a set of internal variables. The derivatives of these hierarchical functions form an orthonormal basis with the property,

$$\int_{-1}^1 \frac{dN_a}{d\xi} \frac{dN_b}{d\xi} d\xi = \delta_{ab} \quad a, b = 3 : p + 1 \quad (15)$$

As a result of this orthogonality property, the local element stiffness matrix is diagonal beyond  $a > 2$ . Stiffness and mass matrices for this element are given in Szabo and Babuska (1991). The element matrices are hierarchic in the sense that the matrix corresponding to  $\mathcal{S}^p$  is embedded in the matrix corresponding to  $\mathcal{S}^{p+1}$ .

### Hierarchic Fourier Basis

Examining the solution to the Helmholtz problem (2), we hypothesize that the introduction of trigonometric basis functions should be a better approximation to the complex exponential solution, compared to the polynomial interpolation used in the Legendre based elements. In this case we investigate hierarchic elements that start with the standard linear nodal shape functions defined in (12) and then add to these in a hierarchical manner internal shape functions defined in terms of the Fourier modes,

$$N_a(\xi) = \frac{2}{(a-2)\pi} \sin((a-2)(1+\xi)\pi/2) \quad a = 3, 4, \dots, p+1 \quad (16)$$

These functions satisfy  $N_a(\pm 1) = 0$  and the orthogonality properties,

$$\int_{-1}^1 N_a N_b d\xi = \frac{2}{(a-2)\pi} \delta_{ab}; \quad \int_{-1}^1 \frac{dN_a}{d\xi} \frac{dN_b}{d\xi} d\xi = \delta_{ab} \quad (17)$$

As a result of this normalization, the local element stiffness matrix is identical to the stiffness matrix obtained with the Legendre polynomial based elements. However, the use of Fourier modes diagonalizes the mass matrix.

### Lagrange basis with Lobatto quadrature

P-type elements based on Lagrange interpolation polynomials in conjunction with Gauss-Lobatto quadrature lead to the so-called ‘spectral elements’ when used with a high spectral order  $p$ , see Patera (1984), Maday and Patera (1989), and Fischer and Patera (1991). These spectral elements are designed to combine the geometric flexibility of the standard finite element techniques with the rapid convergence rate of global spectral schemes, for example Voight, Gottlieb and Hussaini (1984), and Canuto, Hussaini, Quarteroni, and Zang (1988).

In the spectral element method, the solution variable  $\phi^h$  is expanded within each element in terms of high-order Lagrangian interpolants,  $N_a(\xi) \in \mathcal{P}^p$ :

$$\{N_a(\xi) \in \mathcal{P}^p, N_a(\xi_b) = \delta_{ab} \forall a, b \in \{1, \dots, p+1\}\} \quad (18)$$

evaluated at  $p+1$  Gauss-Lobatto points. such that  $\xi_1 = -1$  and  $\xi_{p+1} = 1$ , with the other points being obtained as the roots of the derivative of the Legendre polynomials. Gauss-Lobatto points  $\xi_a$ , and their corresponding weight factors  $W_a$  can be found in tables; see Szabo and Babuska (1991), or computed directly from subroutine libraries; see Canuto, Hussaini, Quarteroni, and Zang (1988). In this case, the solution variables

are all nodal values,  $\phi_a = \phi^h(\xi_a)$ , and the basis is not hierarchical. The element stiffness and mass matrices for these elements are,

$$k_{ab}^e = \frac{2}{h} \sum_{q=1}^{p+1} N'_a(\xi_q) N'_b(\xi_q) W_q \quad (19)$$

$$m_{ab}^e = \frac{h}{2c^2} \sum_{q=1}^{p+1} N_a(\xi_q) N_b(\xi_q) W_q = \frac{h}{2c^2} \delta_{ab} W_a \quad (20)$$

By choice of Gauss-Lobatto quadrature, the elemental mass matrix is underintegrated and diagonal. For one-dimensional elements, the stiffness matrix is exactly integrated by Gauss-Lobatto quadrature. However, for two and three dimensional elements, the stiffness matrix will be underintegrated. Convergence and stability results for these elements can be found in Maday and Patera (1989).

### 3.1 Discrete Fourier decomposition

The complex wavenumber Fourier analysis technique used to investigate the dispersive and attenuation properties of p-type finite elements employs only a minor modification to the technique of real wavenumber analysis but is completely general, and can accommodate any uniform finite element discretization and spectral order.

The frequency dependent dynamic stiffness matrix  $\mathbf{s}^e$  is partitioned into the following matrix block form,

$$\mathbf{s}^e = \begin{bmatrix} \mathbf{s}_{11} & \mathbf{s}_{12} \\ \mathbf{s}_{12}^T & \mathbf{s}_{22} \end{bmatrix} \in \mathbb{R}^{(p+1) \times (p+1)} \quad (21)$$

The matrix partition  $\mathbf{s}_{22} \in \mathbb{R}^{(p-1) \times (p-1)}$  corresponds to interactions among internal shape functions,  $\mathbf{s}_{12} \in \mathbb{R}^{2 \times (p+1)}$  is the coupling matrix partition due to interactions between internal shape functions and nodal shape functions, and finally,  $\mathbf{s}_{11} \in \mathbb{R}^{2 \times 2}$  corresponds to interactions among the nodal shape functions  $N_1$  and  $N_2$ . Using the Schur complement,

$$\mathbf{g}^e = \mathbf{s}_{11} - \mathbf{s}_{12} \mathbf{s}_{22}^{-1} \mathbf{s}_{12}^T, \quad \mathbf{g}^e \in \mathbb{R}^{2 \times 2} \quad (22)$$

we obtain the condensed element dynamic stiffness  $\mathbf{g}^e$  that couples only the two element nodal (i.e. physical) degrees of freedom. For  $p \geq 2$  we obtain  $\mathbf{g}^e$  symbolically using Mathematica, see Wolfram (1991). Consider an infinite uniform mesh with equal element lengths  $h$ . Assembly of the condensed element dynamic stiffness matrices results in a tridiagonal system of linear equations of the form:

$$\mathbf{G}\phi = 0, \quad \mathbf{G} = \mathbf{A}_{e=1}^{n_{el}} \mathbf{g}^e \quad (23)$$

where  $\phi$  is the displacement solution vector, and  $\mathbf{A}$  is the assembly operator. For present purposes, no source terms are included. The  $n$ th equation of this tridiagonal system is a stencil of the form:

$$G_1(\alpha)\phi_{n-1} - 2G_2(\alpha)\phi_n + G_1(\alpha)\phi_{n+1} = 0 \quad (24)$$

All other equations are a repetition of this stencil. In this difference stencil, the coefficients  $G_1(\alpha)$  and  $G_2(\alpha)$  are polynomials of degree  $2p$  in the nondimensional frequency:

$$\alpha = \omega h/c \quad (25)$$

For linear elements ( $p = 1$ ), we recover the difference coefficients of standard consistent and diagonal mass finite element approximations,

$$G_1(\alpha) = 1 + \epsilon\alpha^2/6, \quad G_2(\alpha) = 1 - (3 - \epsilon)\alpha^2/6 \quad (26)$$

The constant  $\epsilon$  is a mass approximation parameter equal to 1 for exactly integrated (consistent) mass, and 0 for Lobatto integrated (diagonal) mass.

The structure of the stencil is seen by writing (24) in the difference operator form,

$$F(\alpha)\phi_n = 0 \quad (27)$$

where,

$$F(\alpha) = \sum_{j=-1}^1 F_j(\alpha)E_j \quad (28)$$

is a second order linear difference operator and  $E_j$  is a shift operator with the property  $E_j\phi_n = \phi_{n+j}$ . The symmetric frequency dependent coefficients are,

$$\begin{aligned} F_1(\alpha) &= G_1(\alpha) = F_{-1}(\alpha) \\ F_0(\alpha) &= -2G_2(\alpha) \end{aligned}$$

In analogy with (2), an exponential solution to (27) is assumed having the form:

$$\phi_n = Ae^{ik^h x_n}, \quad x_n = nh \quad (29)$$

where  $k^h \in \mathbb{C}$  is the numerical wavenumber. Substitution of (29) into (27) results in the characteristic function,

$$\tilde{F}(\alpha, \beta) = \sum_{j=-1}^1 F_j(\alpha)e^{ij\beta} = 0 \quad (30)$$

where  $\tilde{F}(\alpha, \beta)$  may be identified as the discrete Fourier transform of the linear difference operator  $F$ ,  $\alpha$  is the normalized frequency, and  $\beta$  is the normalized wavenumber:

$$\beta = k^h h \quad (31)$$

Due to the symmetric discretization ( $F_1 = F_{-1}$ ), we find that  $\tilde{F}$  is an even function resulting in the wavenumber-frequency relation,

$$\cos(\beta) = \lambda(\alpha) \quad (32)$$

$$\lambda(\alpha) := \frac{G_2(\alpha)}{G_1(\alpha)} \quad (33)$$

where the real spectrum of  $\beta$  is periodic in  $2\pi$  with aliasing,  $\beta = \beta + 2\pi m$ ;  $m$  is a positive or negative integer.

At this point, we depart from the standard finite element dispersion technique in which real frequency roots of (32) are sought for a given real wavenumber. Instead, we seek all the wavenumber roots of (32) for a given real frequency. The complex roots of (32) are found using the complex arc cosine, see Churchill, Brown, and Verhey (1976),

$$Re(\beta) + iIm(\beta) = -i \ln(\lambda(\alpha) + i\sqrt{1 - (\lambda(\alpha))^2}) \quad (34)$$

It is noted that the amplitude of the discrete nodal solution is,

$$|\phi_n| = |A|e^{-iIm(\beta)} \quad (35)$$

where the imaginary part  $Im(\beta)$  is seen to be an attenuation parameter.

## 3.2 Dispersion and attenuation analysis

In this section we discuss the complex wavenumbers that arise from the Fourier analysis of p-version finite elements up to order  $p = 5$ . It will be shown that the finite element characteristic equation (32) admits pure real wavenumbers, (propagating solutions) only when the frequency falls within a finite number of bands called passing bands. The number of passing bands is equal to the spectral order  $p$  of the elements in the mesh. In addition it will be shown that there are  $p$  stopping bands where the wavenumbers are complex.

### 3.2.1 Low-order elements

For  $p = 1$  there is only one passing band where the wavenumber is purely real. For frequencies lower than a limiting frequency called the cut-off frequency we obtain real solutions for  $\beta$ . The cut-off frequency for consistent mass is  $\alpha_{max} = \sqrt{12}$  and for diagonal mass  $\alpha_{max} = 2$ . In the complex wavenumber plane, for frequencies below the cut-off, then  $|\lambda| < 1$ , and the characteristic equation is satisfied by,

$$Re(\beta) = \cos^{-1}(\lambda), \quad \text{and} \quad Im(\beta) = 0 \quad (36)$$

For higher frequencies  $\beta$  is complex, since above the cut-off frequency,  $|\lambda| > 1$ , and the characteristic equation is satisfied by,

$$Re(\beta) = \pi, \quad \text{and} \quad Im(\beta) = \cosh^{-1}(\lambda) \quad (37)$$

Figure 1 plots the frequency dependence of the real (propagating) and imaginary (decaying) components of the complex numerical wavenumber  $k^h \in \mathbb{C}$ . In this Figure, the normalized frequency ( $\omega h/c$ ) is the independent variable and the normalized wavenumber ( $k^h h$ ) is the dependent variable.

The real wavenumber corresponding to the cut-off frequency is called the spatial resolution limit. For  $p = 1$ , the limit of spatial resolution is two elements per wavelength or  $Re(\beta) = \pi$ . For frequencies between 0 and  $\alpha_{max}$ ,  $\beta$  is real, and for frequencies above the cut-off, the real part of the discrete wavenumber stays constant at  $Re(\beta) = \pi$ , while the imaginary part of the discrete wavenumber increases rapidly.

As a result, the amplitude from node to node along the mesh stays constant until the frequency reaches the cut-off. Above the cut-off the amplitude decays exponentially along the mesh,

$$\left| \frac{\phi_{n+1}}{\phi_n} \right| = \begin{cases} 1 & \alpha < \alpha_{max} \\ e^{-Im(\beta)} & \alpha > \alpha_{max} \end{cases}$$

Figure 2 plots this amplitude spectrum. This illustrates how the finite element mesh acts as a low-pass filter analogous to discrete signal processing of data – allowing propagation of all frequencies up to the cut-off frequency, while strongly attenuating frequencies above the cut-off frequency.

### 3.2.2 Higher-order elements

For a uniform mesh of  $p$ -version finite elements with spectral order ( $p = 2$ ), the frequency dependence of the real and imaginary parts of  $k^h \in \mathbb{C}$  are plotted in Figure 3. In this case, there are two passing bands: one for frequencies between  $0 < \alpha < \alpha_1$  and one for frequencies between  $\alpha_2 < \alpha < \alpha_{max}$ . Within these bands, there is a purely propagating solution with  $|\lambda| < 1$  and the characteristic equation is satisfied by,

$$Re(\beta) = \cos^{-1}(\lambda), \quad \text{and} \quad Im(\beta) = 0 \quad (38)$$

The dispersion curve in the lower passing band is called the acoustical branch and the upper passing band is referred to as the optical branch. These designations arise from the analogous branches found in a diatomic crystal lattice where the frequencies in the lower branch are of the same order of magnitude as acoustical or subsonic vibrations, and frequencies in the upper branch are of the order of magnitude of infrared frequencies, see Brillouin (1953). For our discussions, we use these designations for the different branches, but attach no physical significance to their names.

In the frequency range between these two passing bands,  $\alpha_1 \leq \alpha \leq \alpha_2$ , there is one frequency band where the numerical wavenumbers are complex. In this band,  $|\lambda| > 1$  and the characteristic equation is satisfied by,

$$Re(\beta) = \pi, \quad \text{and} \quad Im(\beta) = \cosh^{-1}(-\lambda) \quad (39)$$

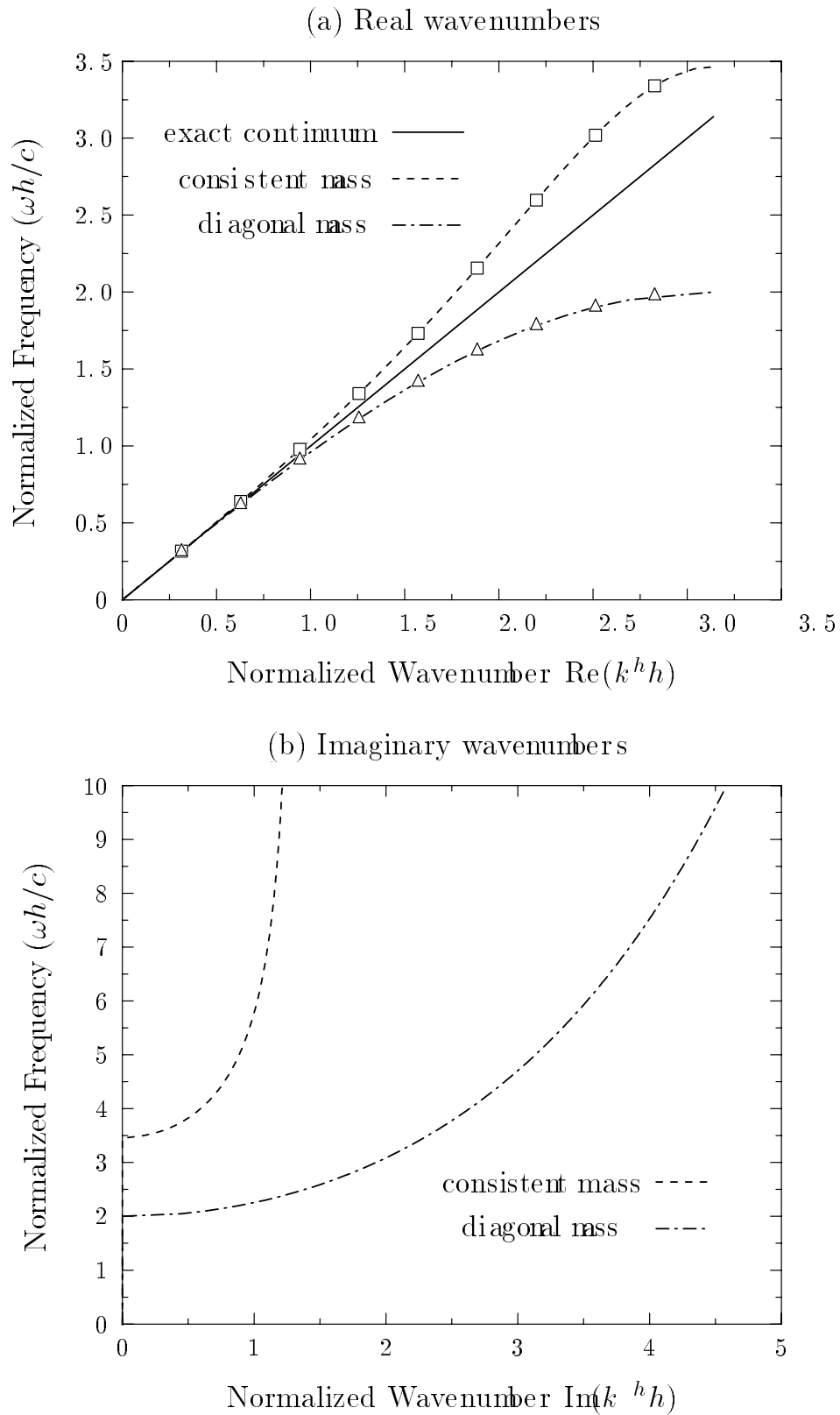


**Fig. 1:** Frequency spectrum comparing linear finite element approximations: (a) Real wavenumbers, (b) Imaginary wavenumbers

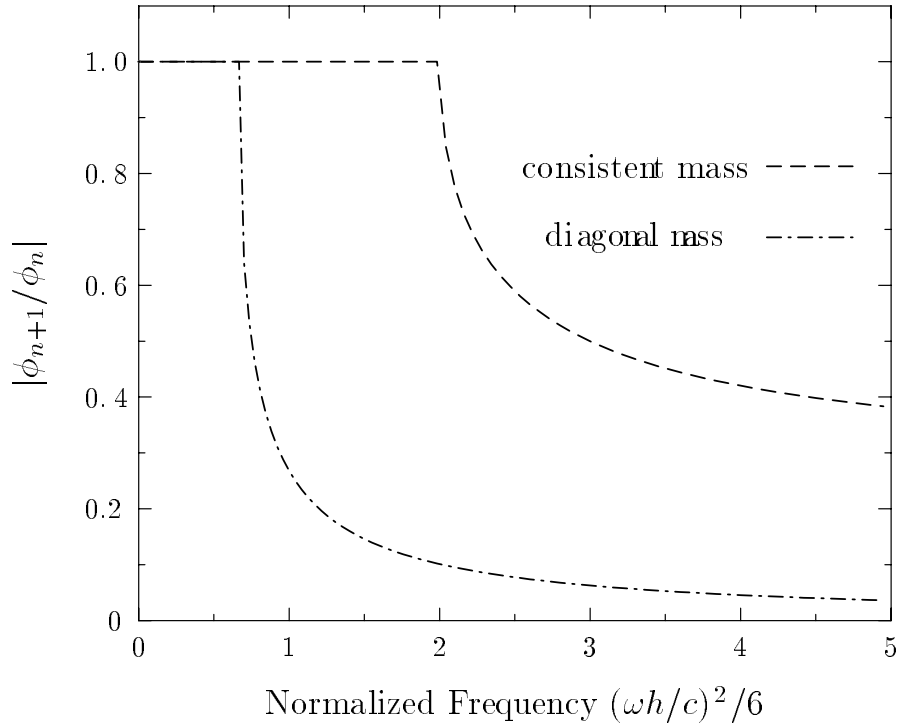


**Fig. 2:** Amplitude spectrum for linear finite elements

This complex wavenumber band is called a stopping band because in this frequency range, the real part of the wavenumber is constant and the imaginary component results in an attenuated wave solution with an amplitude decay proportional to the exponential of the imaginary wavenumber.

Above the cut-off frequency,  $\alpha > \alpha_{max}$ ,  $\lambda > 1$  and the characteristic equation is satisfied by,

$$Re(\beta) = 2\pi, \quad \text{and} \quad Im(\beta) = \cosh^{-1}(\lambda) \quad (40)$$

In this case, the solution propagates with a fixed wavelength equal to the limit of resolution – one quadratic element per wavelength or  $Re(\beta) = 2\pi$  with strong exponential amplitude decay from node to node along the mesh.

The amplitude spectrum for  $p = 2$  is plotted in Figure 4. The amplitude ratio is constant in the first passing band (acoustical branch) up to the complex wavenumber band where the imaginary wavenumber components produce an amplitude decay. In the stopping band, the amplitude is attenuated until a minimum is reached and then increases back up to the exact ratio of one. The amplitude ratio continues to be exact throughout the second passing band (optical branch) until it reaches the cut-off where it is strongly attenuated. The maximum error for Spectral elements is 25 percent while that of the Legendre and Fourier elements is only 10 percent. In addition, the cutoff frequency for the Spectral element falls well below that of the Legendre and Fourier elements.

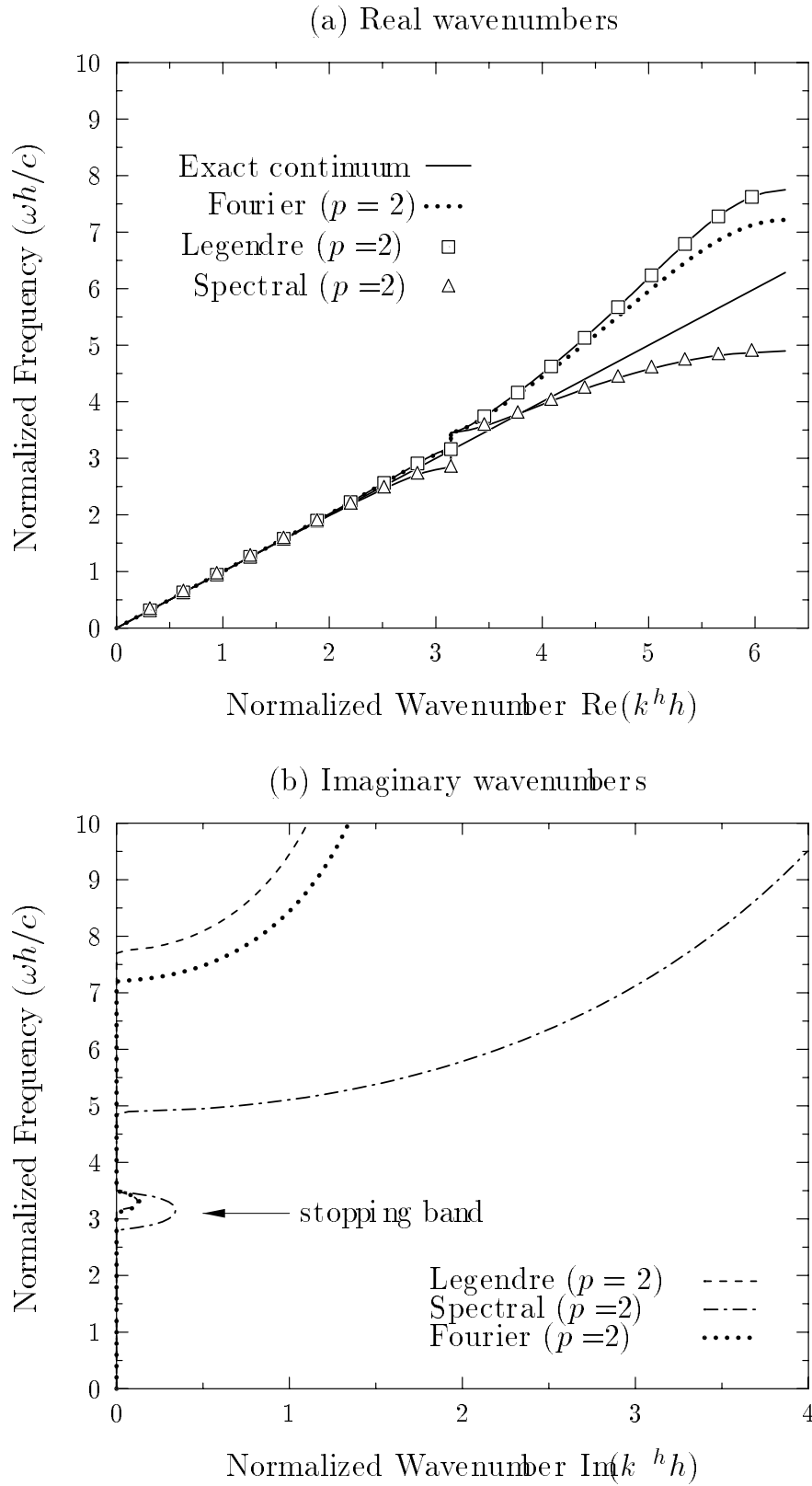


**Fig. 3:** Frequency spectrum comparing quadratic finite element approximations: (a) Real wavenumbers, (b) Imaginary wavenumbers

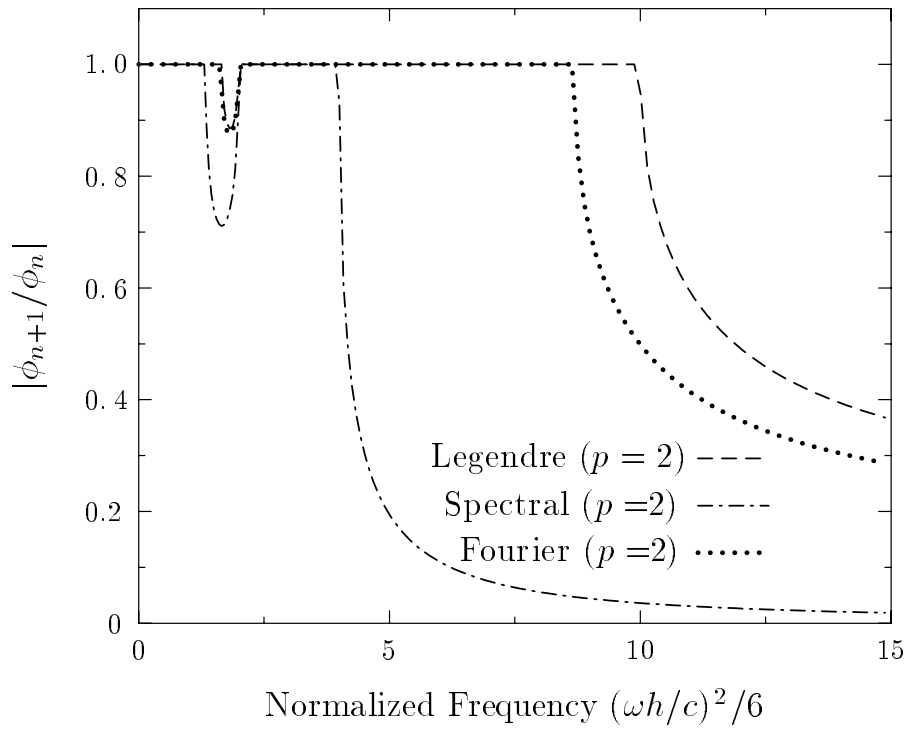


**Fig. 4:** Amplitude spectrum for quadratic elements

Again invoking the signal processing analogy, the character of this amplitude spectrum illustrates how the  $p$ -version finite element mesh acts as a band-pass filter – allowing propagation of all frequencies in the passing bands, while weakly attenuating frequencies in the complex wavenumber band, and strongly attenuating frequencies above the cut-off frequency.

As the spectral order is increased to  $p = 3$ , the spatial resolution limit extends to  $Re(\beta) = 3\pi$ . Figure 5 shows that there are 3 passing and 3 stopping bands present in the frequency spectrum. The first complex wavenumber band occurs when  $Re(\beta) = \pi$ . The frequency range for the first stopping band is very small and appears as a small perturbation in the frequency curve for the imaginary wavenumber component at approximately  $\alpha = \pi$ , see Figure 5. The second stopping band occurs when the real wavenumber component reaches  $2\pi$  and is much larger, with large imaginary wavenumber components present.

As a result of these complex wavenumber bands, we observe the amplitude attenuation characteristics shown in Figure 6. The amplitude ratio is again constant in the passing bands up to the first complex wavenumber band, where there is a very small attenuation loss. Isolating this frequency region in Figure 7, we observe that the maximum amplitude error is only 2.5 percent for the Spectral elements and only 1 percent for Legendre and Fourier elements. Thus in this first complex wavenumber region waves propagate with constant wavenumber  $Re(\beta)$  and only a very small

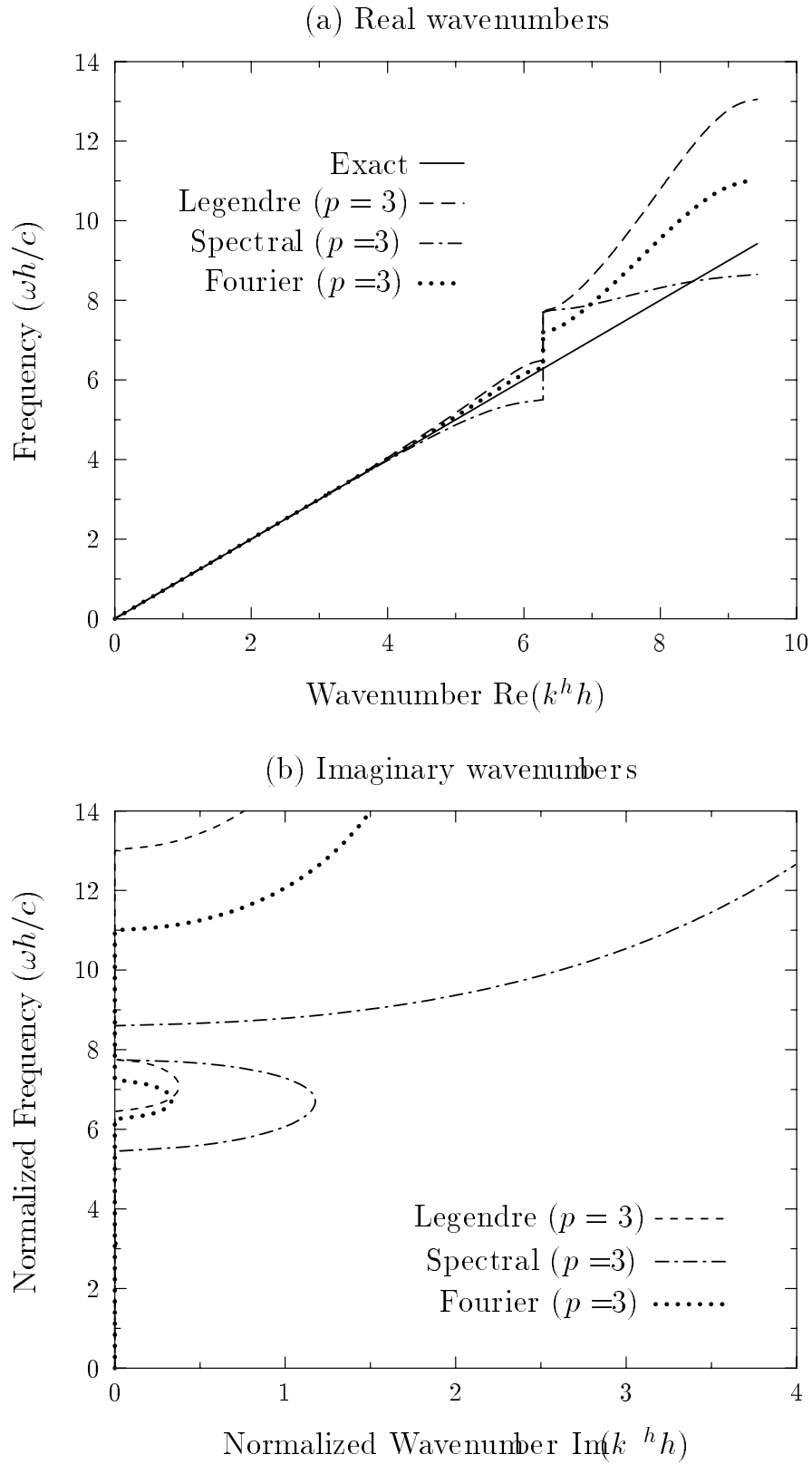


**Fig. 5:** Frequency spectrum comparing cubic finite element approximations: (a) Real wavenumbers, (b) Imaginary wavenumbers

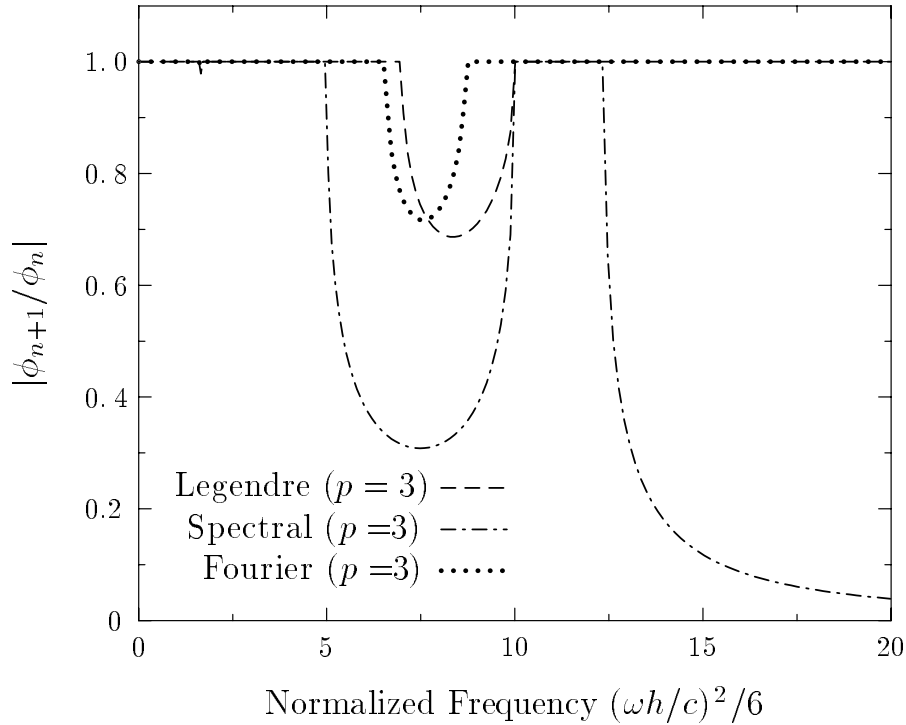


**Fig. 6:** Amplitude spectrum for cubic elements

amplitude decay. The amplitude attenuation in the second complex frequency band is very large and in practice the element size  $h$  should be chosen to avoid this nondimensional frequency range. These observations are extended to higher spectral orders as well. Results for spectral orders  $p = 4$  and  $p = 5$  are shown in Figure 8 and Figure 9 respectively. For nondimensional frequencies up to  $\alpha = (p - 2)\pi$ , the dispersion curves approximate the exact line with slope one. As the nondimensional frequency increases, the Legendre and Spectral elements exhibit loss of accuracy in the upper two optical branches. In contrast, the Fourier element maintains accuracy up to  $\alpha = (p - 1)\pi$ .

In conclusion, the following dispersive properties are observed: (1) There are  $p$  passing bands and  $p$  stopping bands, (2) the limit of resolution occurs at  $Re(\beta) = \pi p$ . In addition, the amplitude attenuation in the first few complex wavenumber (stopping) bands is very small and converges in the limit of large spectral orders to the exact amplitude ratio of one. Thus for large spectral orders the first few stopping bands are not of practical significance. As a general trend we observe that the amplitude error is greater for the Spectral elements than the Legendre and Fourier elements and the cutoff for Spectral elements always occurs before that of Legendre elements.

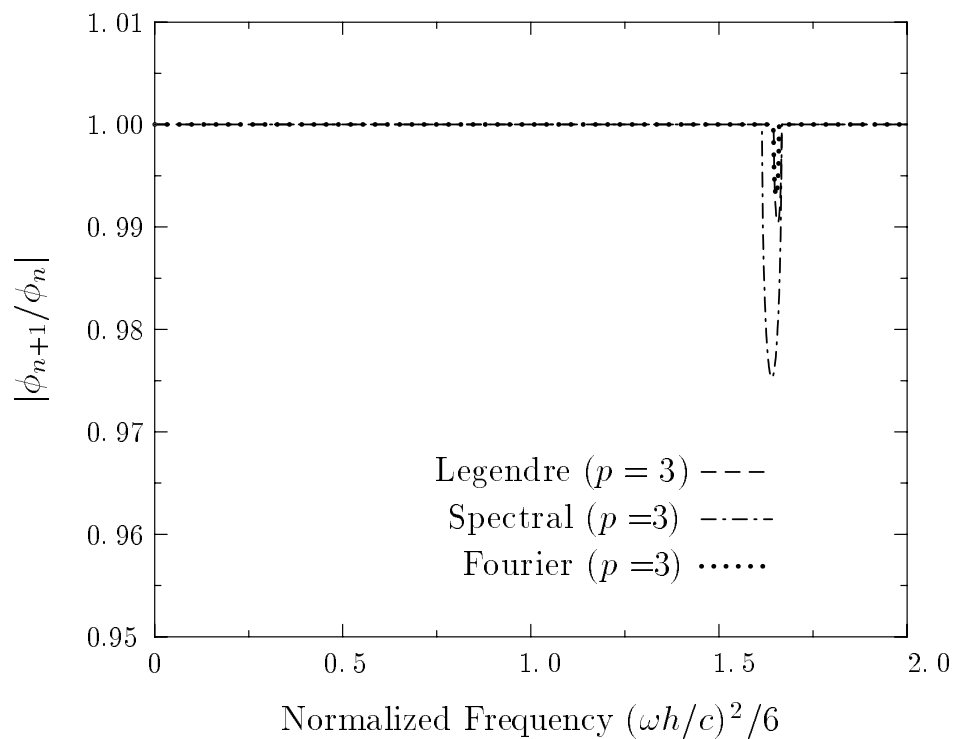


**Fig. 7:** Isolation of amplitude spectrum near first complex wavenumber band

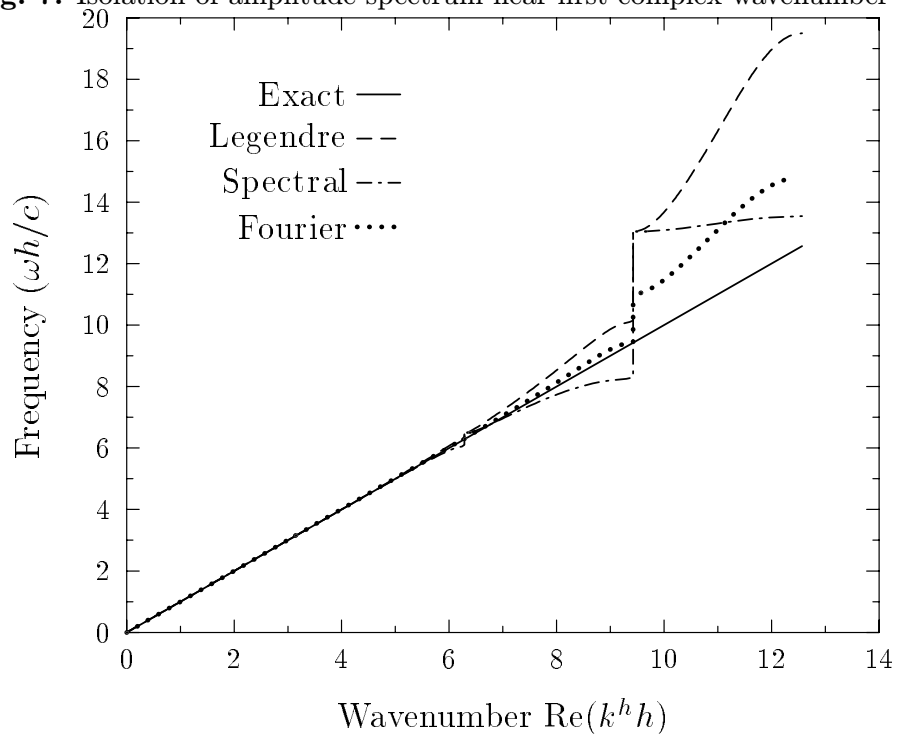


**Fig. 8:** Frequency spectrum for ( $p=4$ ) finite elements: Real wavenumbers

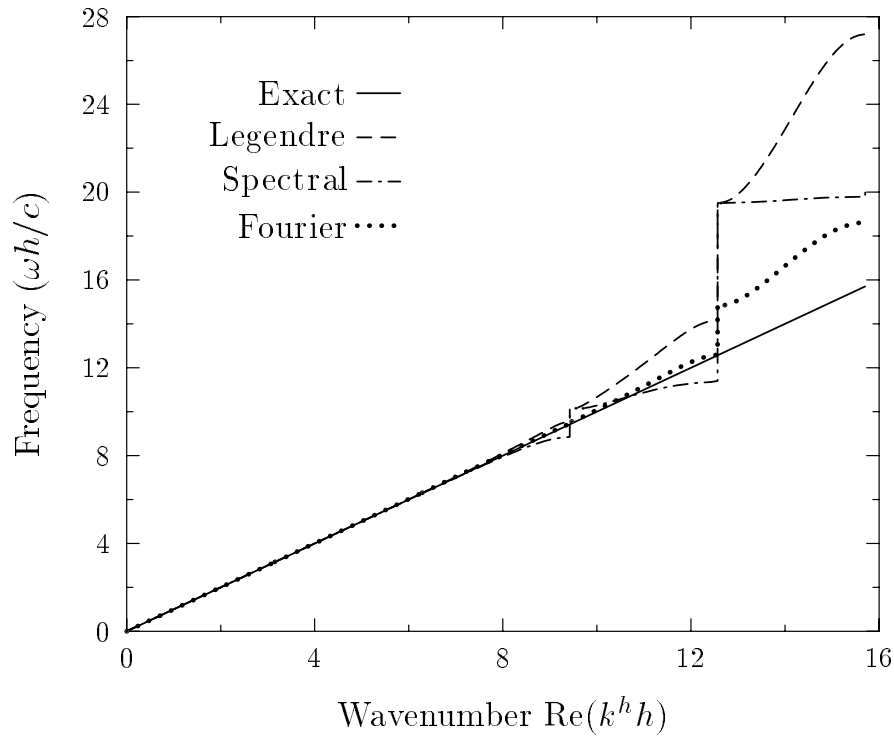


**Fig. 9:** Frequency spectrum for ( $p=5$ ) finite elements: Real wavenumbers

### 3.2.3 Analysis of phase error

A comparison of the characteristic equation for the continuum case with that of the discrete case enables us to assess the phase accuracy of  $p$ -type finite elements. Figures 10 through 12 show the phase accuracy of the finite element approximation versus a nondimensional real wavenumber ( $\beta/\pi p$ ). By dividing the wavenumber by the spectral order  $p$  we are able to get an equitable comparison between the methods with the same number of degrees of freedom per wavelength. Throughout the acoustic branch, the phase error converges to the exact solution as the spectral order is increased. Clearly, in the practical range  $0 \leq k^h h/\pi p \leq .5$  the higher-order  $p$ -type elements exhibit increased accuracy compared to low-order finite elements, for the same number of degrees of freedom.

In the optical branches, the dispersive errors increase. For hierarchical Legendre and Fourier elements we observe that  $c^h/c = k/k^h > 1$  which implies a phase lead over the entire wavenumber spectrum. In contrast, as we increase the normalized wavenumber for spectral elements the phase changes from a phase lag up to the first stopping band where it jumps to a phase lead and then gradually reverts back to a phase lag. We also observe that the use of trigonometric shape functions in the Fourier elements decreases the phase error found in the optical branch as compared to the Legendre case.

The spectral convergence rate of the phase error is observed by fixing the nondi-

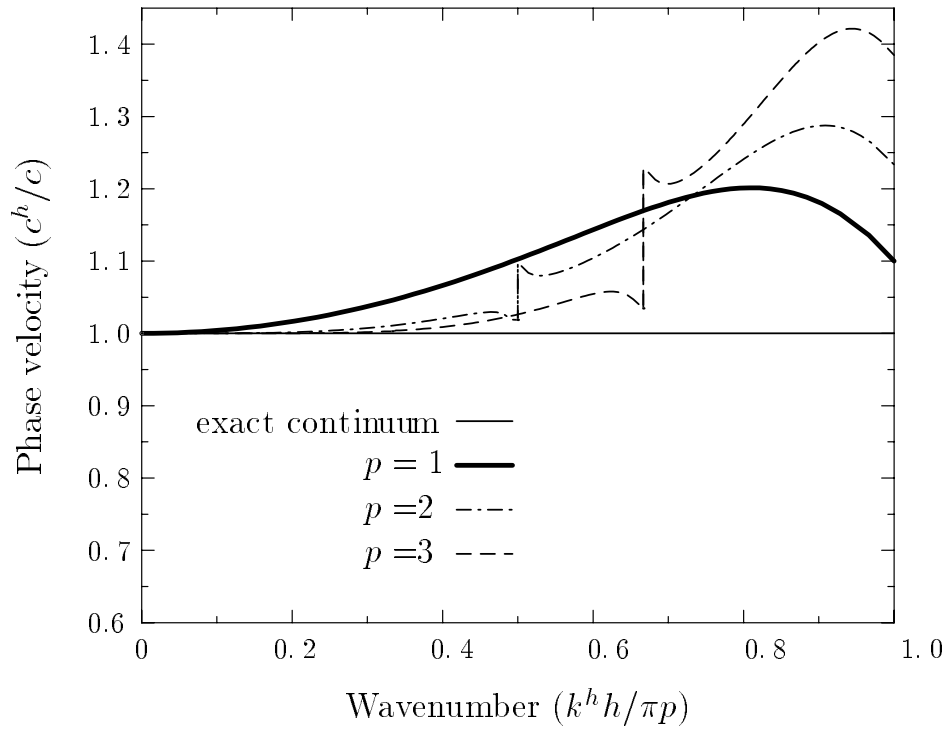


**Fig. 10:** Phase velocity error for Legendre elements with polynomial orders  $p=1,2,3$

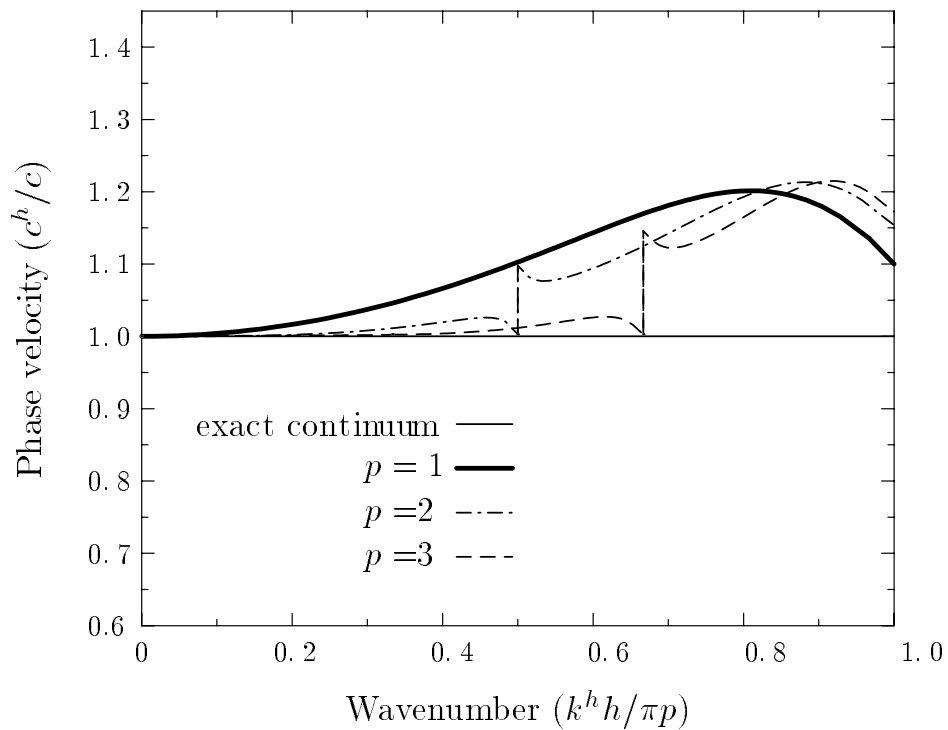


**Fig. 11:** Phase velocity error for Fourier elements with trigonometric orders  $p=1,2,3$

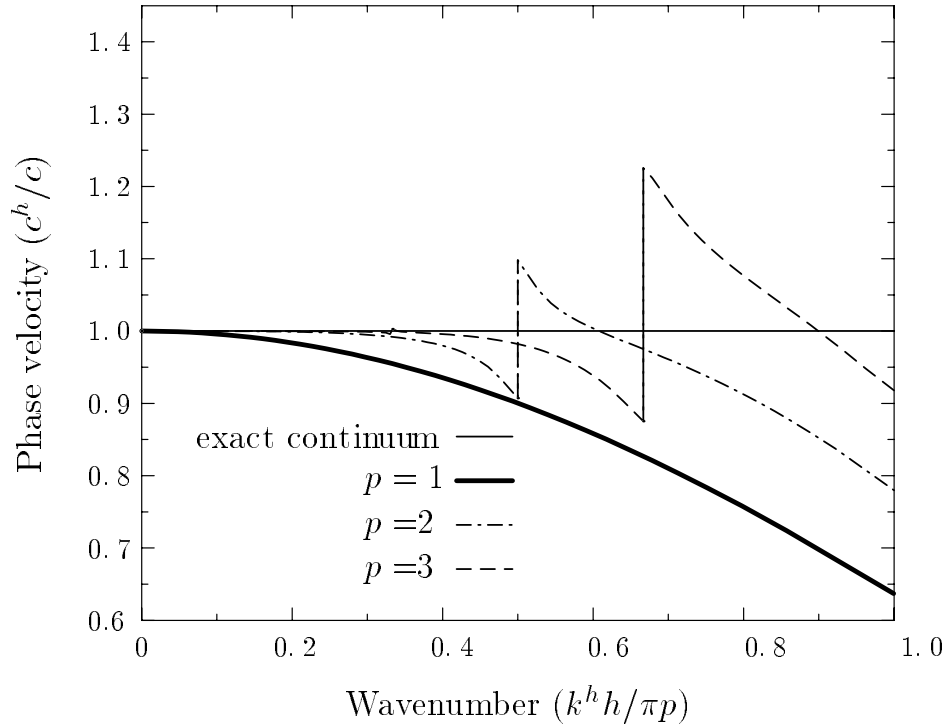


**Fig. 12:** Phase velocity error for Spectral elements with polynomial orders  $p=1,2,3$

mensional wavenumber at  $kh/p = \pi/5$ . This wavenumber corresponds to ten elements per wavelength divided by the spectral order. The results are given in Table 1 for Legendre and Spectral elements up to order  $p = 5$ . Results for Fourier elements are similar to Legendre elements.

**Table 1:** Phase error (percent) for fixed  $kh/p = \pi/5$

p	Legendre	Spectral
1	1.60e-00	-1.69e-00
2	1.59e-01	-9.17e-02
3	1.96e-02	-7.50e-03
4	2.63e-03	-9.60e-04
5	3.69e-04	6.58e-03

The convergence rate of  $p$ -type elements is investigated further by examining the phase as the number of solution variables per wavelength is increased. For example for  $p = 1$  a Taylor series expansion of the dispersion relation (32) gives,

$$k^h h = \alpha \pm \frac{(\alpha)^3}{24} + \frac{3(\alpha)^5}{640} \pm \mathcal{O}(\alpha)^7 \quad (41)$$

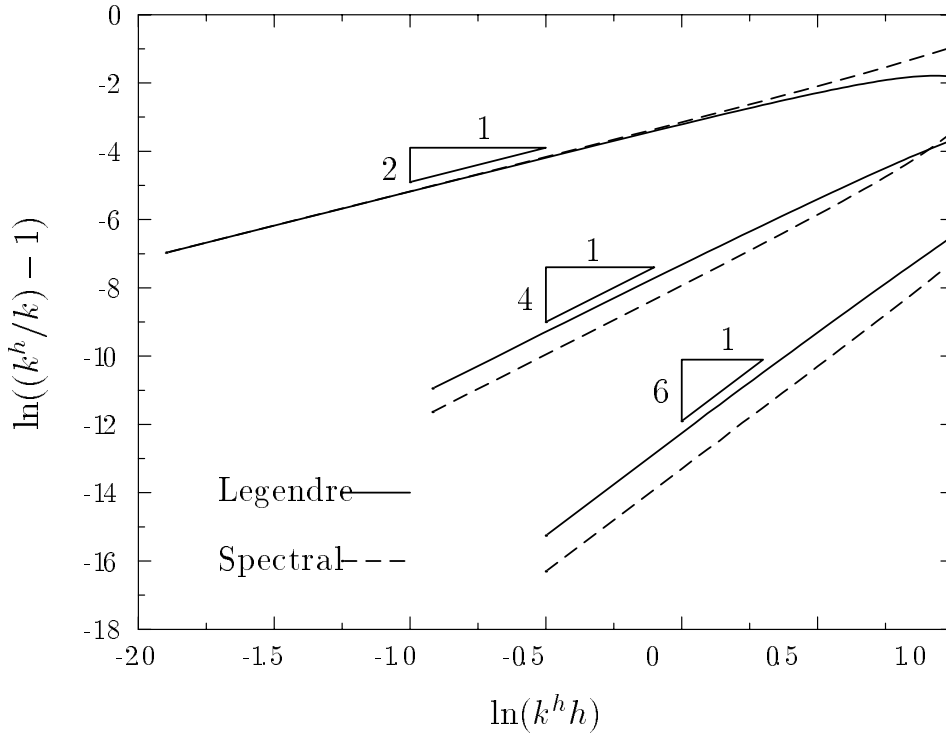


**Fig. 13:** Convergence of phase error with polynomial orders  $p=1,2,3$

where the plus sign is for diagonal mass and the minus sign for consistent mass. Thus for diagonal mass the discrete solution has a phase lag  $k^h \geq k$ , while for consistent mass the discrete solution has a phase lead  $k^h \leq k$ . From this expansion we find that the finite element nodal solution is locally second order accurate. In general, in the range of resolution, the phase error for spectral order  $p$  is of the order,

$$\frac{k^h}{k} - 1 = \mathcal{O}(kh)^{2p} \quad (42)$$

with the nodal solution for the displacement,

$$\phi_n = Ae^{ikx_n[1 \pm \mathcal{O}(kh)^{2p}]} \quad (43)$$

This result is verified for spectral orders of  $p = 1, 2, 3$  in Figure 13, where the slope of the lines show the rate of convergence of the phase error to be  $2p$ . For reference, we note that 10 elements per wavelength corresponds to -1.0 on the abscissa of this plot.

For  $p = 1$ , if  $k^3h^2$  is assumed small in a fixed region in  $x$ , then Bayliss and Goldstein and Turkel (1985) have shown that the error measured in the  $L_2$  norm is,

$$\|e_n\|_{L_2} = \mathcal{O}(k^3h^2)\|\phi\|_{L_2} \quad (44)$$

with an error bound  $\mathcal{O}(k^2h)$  in the  $H^1$  norm. Thus, discretization errors when measured in the norms  $L_2$  and  $H^1$  grow as  $k$  increases even though the number of elements per wavelength remains fixed ( $kh = \text{constant}$ ).

### 3.2.4 Analysis of attenuation

Although the amplitude from node to node is exact for frequencies within the passing bands, it is possible for the p-type finite element solution to exhibit amplitude attenuation at points internal to physical nodes. Analysis of amplitude attenuation at points internal to the physical nodes is investigated by examining quadratic elements of order  $p = 2$ . In this case, the dynamic stiffness matrix (10) is assembled without condensation and the internal variable is written in terms of the center point. The resulting stencils related to equations  $n$  and  $n \pm 1/2$  are of the form,

$$S = (K - \alpha^2 M)\phi = 0 \quad (45)$$

where  $K$  and  $M$  are  $(2 \times 5)$  stiffness and mass difference equations and

$$\phi^T = ( \phi_{n-1} \quad \phi_{n-1/2} \quad \phi_n \quad \phi_{n+1/2} \quad \phi_{n+1} ) \quad (46)$$

Allowing for different amplitudes at the exterior nodes  $n$ , and element center nodes  $n \pm 1/2$  we assume the complex exponential solutions,

$$\phi_n = A_1 e^{i\beta(n)} \quad (47)$$

$$\phi_{n+1/2} = A_2 e^{i\beta(n+1/2)} \quad (48)$$

Substitution of the above two solutions into (45) results in the symmetric characteristic matrix,

$$\tilde{S}(\alpha, \beta) = \begin{bmatrix} \tilde{S}_{11} & \tilde{S}_{12} \\ \tilde{S}_{12} & \tilde{S}_{22} \end{bmatrix} \begin{Bmatrix} A_1 \\ A_2 \end{Bmatrix} = \mathbf{0} \quad (49)$$

Solving this system, the amplitude ratio  $r = A_2/A_1$  is,

$$r(\alpha, \beta) = -\frac{\tilde{S}_{12}(\alpha, \beta)}{\tilde{S}_{22}(\alpha, \beta)} = -\frac{\tilde{S}_{11}(\alpha, \beta)}{\tilde{S}_{12}(\alpha, \beta)} \quad (50)$$

Note that the dispersion relation found earlier in (32) is obtained by setting the characteristic matrix to zero,  $\det \tilde{S} = \tilde{F}(\alpha, \beta) = 0$ .

Figure 14 shows the amplitude ratio  $r = A_2/A_1$  plotted as a function of wavenumber. The curves lying above the ratio of one are acoustical branches, while those below are optical branches. In the range  $0 \leq \beta \leq 2\pi/3$ , the amplitudes are nearly equal to the exact value of one. Near the stopping band,  $\beta = \pi$ ,  $r$  increases rapidly. At  $\beta = \pi$ , the amplitude ratio skips to the optical branch where it assumes the value zero. In the optical branch the ratio tends to the limit  $r = 0.5$ . The physical interpretation of this result is discussed at length in Brillouin (1953): Here we emphasize that two alternative interpretations are possible. Referring to (48), the solution for the finite element mesh can be represented as *two waves*, one propagating along the exterior

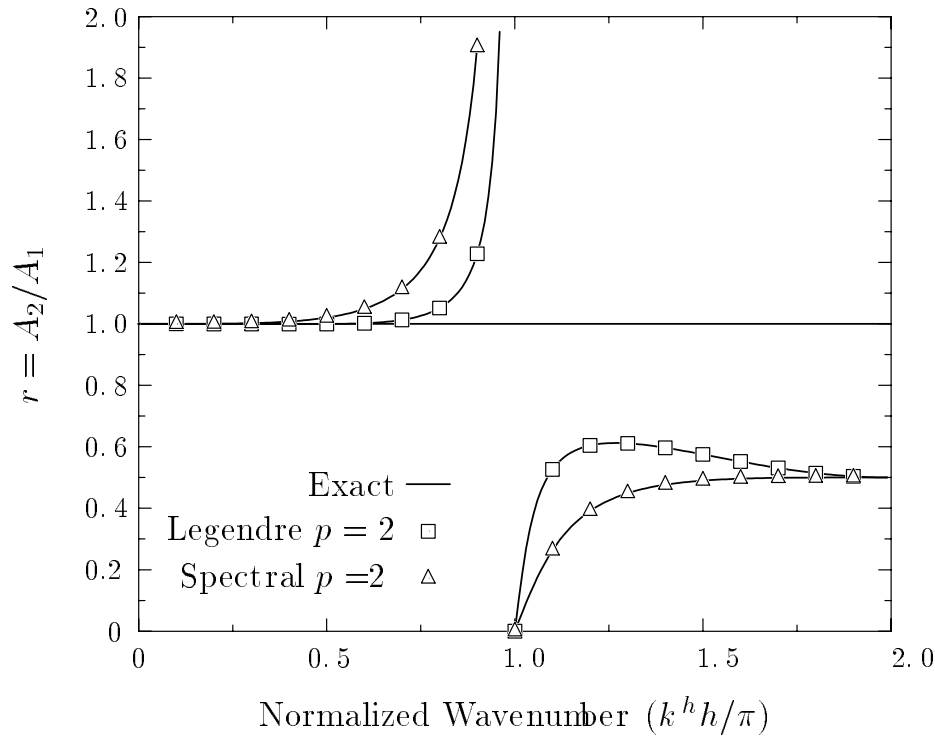


**Fig. 14:** Amplitude spectrum for quadratic elements at interior nodes

nodes  $n$ , and the other propagating along the interior points  $n \pm 1/2$ . An alternative representation is a *single wave* propagating through both interior and exterior points,

$$\phi_m = C_+ e^{i(\bar{\beta})m} + C_- e^{i(\bar{\beta}-\pi)m} \quad (51)$$

where  $\beta = 2\bar{\beta}$  and  $C_+ = (A_1 + A_2)/2$  and  $C_- = (A_1 - A_2)/2$ . This solution describes the superposition of two waves propagating in opposite directions with wavenumbers  $\bar{\beta}$  to the right and  $\bar{\beta} - \pi$  to the left. The wave propagating to the right is partially reflected as it traverses each node, thus giving rise to a solution that consists of both a transmitted and a reflected wave component. The physical significance of this result is that while the amplitude is exact from node to node for frequencies within passing bands, the reflected wave component causes amplitude attenuation at internal points.

For quadratic Legendre elements, amplitude attenuation is insignificant for  $k^h h < 2\pi/3$  ( three elements per wavelength), while for quadratic Spectral elements amplitude attenuation is insignificant for  $k^h h < \pi/2$  ( four elements per wavelength). Results for Fourier elements are similar to the Legendre elements.

## 4 Example Problem: Dirichlet–Fixed Bar

By allowing for complex wavenumbers, a more complete characterization of the stopping bands in the frequency spectrum of finite element discretizations has been pre-

sented. By studying the closed form p-type finite element solution of a canonical steady-state vibration problem, the role that complex wavenumbers play in the practical solution of physical boundary value problems is revealed.

Consider the steady-state vibration problem of a bar of length  $L$ ,

$$\frac{d^2\phi}{dx^2} + k^2\phi = 0, \quad \phi(0) = \bar{\phi}, \quad \phi(L) = 0 \quad (52)$$

Assuming a complex wave solution,

$$\phi(x) = A_+e^{ikx} + A_-e^{-ikx} \quad (53)$$

the wave representation of the solution to (52) may be obtained as,

$$\phi(x, \omega) = \bar{\phi} \frac{\sin(k(L-x))}{\sin(kL)} \quad (54)$$

This response becomes unbounded at the eigenvalues  $\sin kL = 0$ , i.e.

$$k_j = j\pi/L \quad j = 1, 2, \dots, \infty \quad (55)$$

Now consider the bar discretized with  $N$  uniformly spaced elements of length  $h$ .

$$0 = x_0 < x_1 < \dots < x_{N-1} < x_N = L = Nh$$

After condensation of internal variables, the finite element equations are in symmetric tridiagonal form of order  $(N-1)$  with band,

$$G_1\phi_{n-1} - 2G_2\phi_n + G_1\phi_{n+1} = 0 \quad n = 1 : N-1 \quad (56)$$

It may be shown that the solution of (56), subject to the boundary conditions  $\phi_0 = \bar{\phi}$  and  $\phi_N = 0$  is given by,

$$\phi^h(x_n, \omega) = \bar{\phi} \frac{\sin(k^h(L-x_n))}{\sin(k^hL)} \quad n = 0 : N \quad (57)$$

where  $k^h$  is the numerical wavenumber defined in (32) and  $L = Nh$  and  $x_n = nh$ . This closed form nodal solution is valid for any of the p-type elements discussed previously and for any spectral order  $p$ . Comparing the closed form finite element solution with the analytical solution (54), it is clear that the wave representations of the response are identical except that  $k$  has been replaced by  $k^h$ . The important point here is that this wave solution consists of the same numerical wavenumbers present for the infinite rod found by our Fourier analysis except that both outgoing and incoming waves are present. The following analysis establishes the role of complex wavenumbers in the finite element solution of practical boundary value problems.

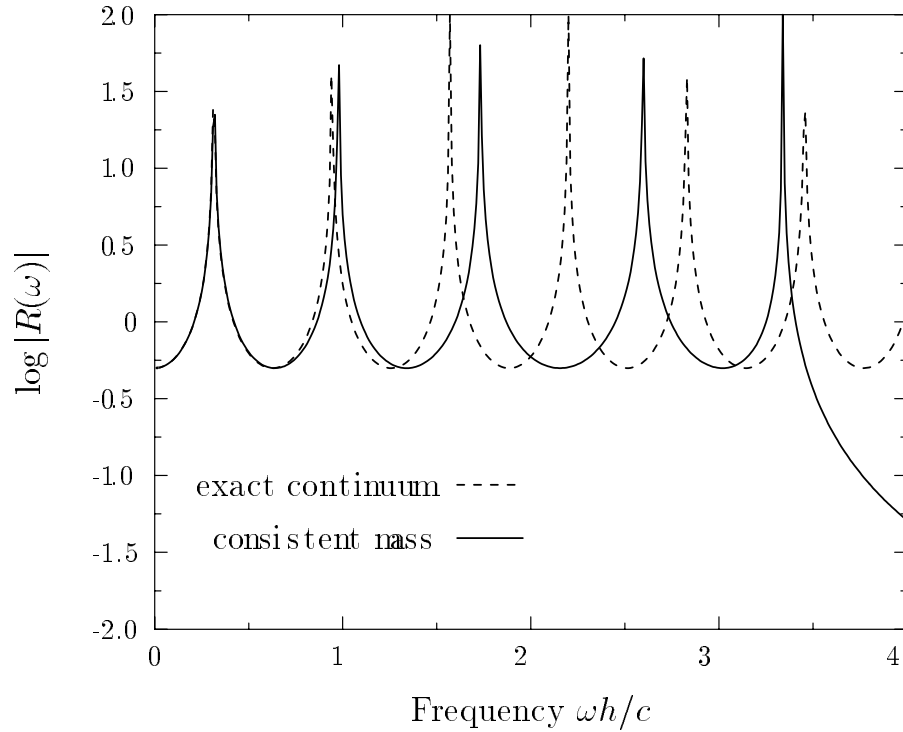


**Fig. 15:** Frequency response spectrum for Dirichlet-Fixed rod using consistent mass linear element

## 4.1 Frequency response spectrum

The existence of the cut-off frequency and stopping bands for the example problem is exposed from the frequency response spectrum. The dispersive and attenuation characteristics are investigated using the frequency response function obtained from the wave solution (57) and a uniform mesh of ten ( $N = 10$ ) p-type elements.

### 4.1.1 Low-order elements

Figures 15 and 16 show the frequency response spectrum at the midnode using linear elements ( $p = 1$ ) with consistent and diagonal mass approximations respectively.

$$R(\omega) = \phi^h(x_5, \omega) / \bar{\phi} \quad (58)$$

The sharp peaks indicate the position of the resonant frequencies of the vibration problem. Excellent agreement with the exact response is obtained for both mass discretizations up to the practical limit of resolution of approximately ten elements per wavelength ( $\omega h/c \approx \pi/5$ ). These figures also display the considerable errors that are present in the higher modes. The phase lead present using consistent mass and the phase lag present using diagonal mass is also exposed in these results. Existence of the cutoff frequency is evident by the sharp drop in the response at  $(\omega h/c) = \sqrt{12}$  for consistent mass and at  $(\omega h/c) = 2$  for diagonal mass.

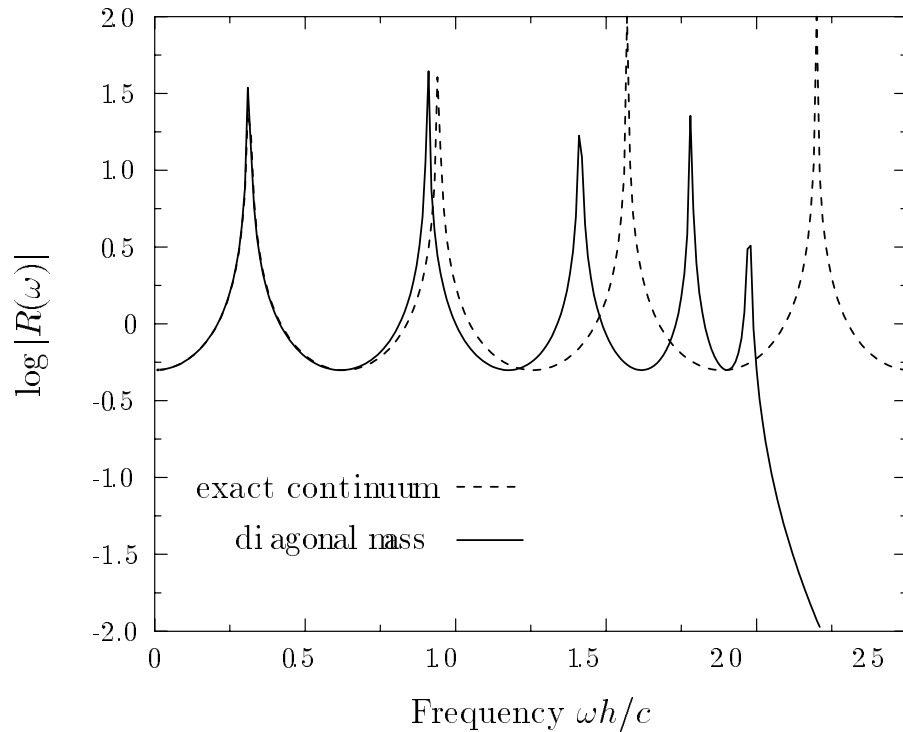


**Fig. 16:** Frequency response spectrum for Dirichlet-Fixed rod using diagonal mass linear element

#### 4.1.2 Higher-order elements

Figures 17 and 18 show the frequency response at the midnode for a uniform mesh of ten quadratic ( $p = 2$ ) elements. In this case the number of odd modes (resonant peaks) has doubled and the cut-off frequency has been extended. Accurate results are obtained throughout the acoustic branch while considerable errors are present in the optical branch. Up to the stopping band, the solution is more accurate compared to the linear element discretization for the same number of degrees of freedom. For linear elements, the practical limit of accurate solutions is ten elements per wavelength, while for quadratic elements, as few as three elements per wavelength are needed to obtain accurate results. The existence of the stopping band (complex wavenumber band) is evident by the decrease in amplitude response at  $(\omega h/c) \approx \pi$ . The important observation is the direct connection between the frequency response and the complex wavenumber Fourier analysis — the results obtained here are precisely those predicted by the Fourier analysis.

In Figure 19, we observe the character of the response in the stopping band by plotting the solution (57) with normalized frequency corresponding to the maximum imaginary wavenumber component in the complex band. The amplitude decay as the waves pass through the finite element mesh is displayed. It is clear that the response has a propagating component fixed at  $Re(k^h h) = \pi$  corresponding to two elements per

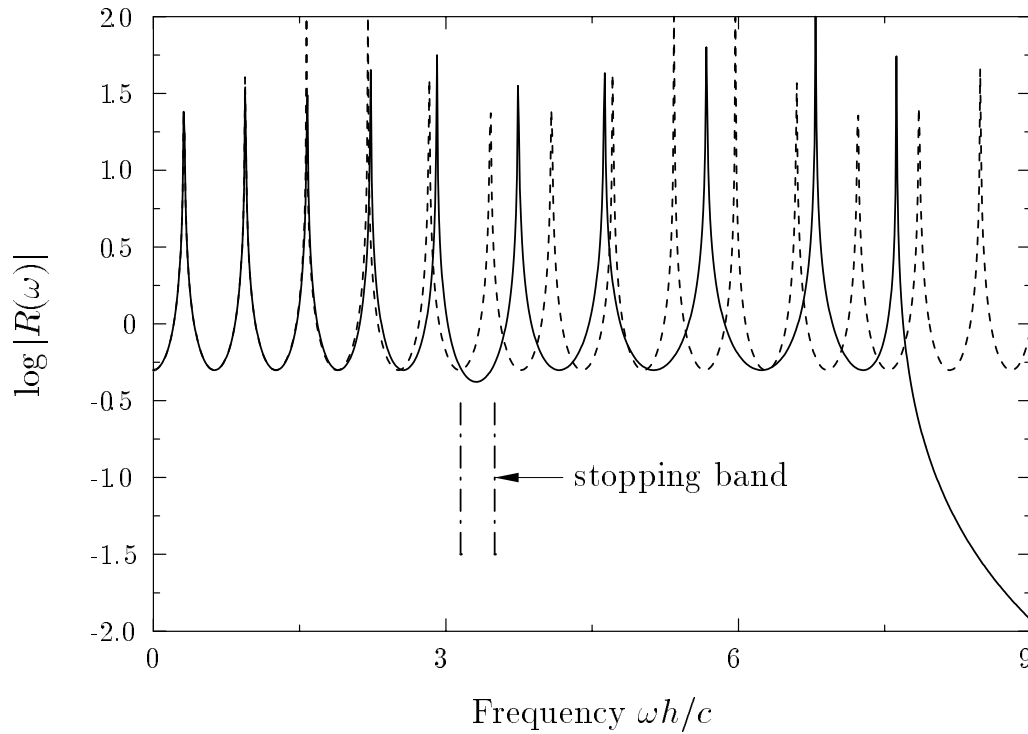


**Fig. 17:** Frequency response spectrum for Dirichlet-Fixed rod using quadratic Legendre elements

wavelength, while the imaginary component manifests itself in the amplitude decay.

## 4.2 Discrete eigenvalues

A deeper understanding of the connection between the complex Fourier analysis and dispersion results obtained from the finite element solution of boundary value problems is obtained by investigating the eigenfrequencies (resonant peaks) present in the example problem. In this case, real frequency roots (eigenvalues) are sought corresponding to real wavenumbers (eigenmodes). Since the eigenmodes are all real for this problem, the eigenvalues fall below the cut-off frequency and outside the complex wavenumber stopping bands.

For the continuous bar, the eigenmodes  $k_j = j\pi/L$  are linearly proportional to the eigenvalues through the dispersion relation (4):

$$\omega_j h/c = k_j h \quad (59)$$

The real eigenmodes for a uniform mesh of  $p$ -version finite elements of any spectral order are,

$$k_j^h = j\pi/L \quad j = 1 : pN - 1 \quad (60)$$

Comparing this result to (55) we find that the eigenmodes for the finite element mesh are exact, i.e.  $k_j^h = k_j$ , up to the number of free variables ( $pN - 1$ ) present in the

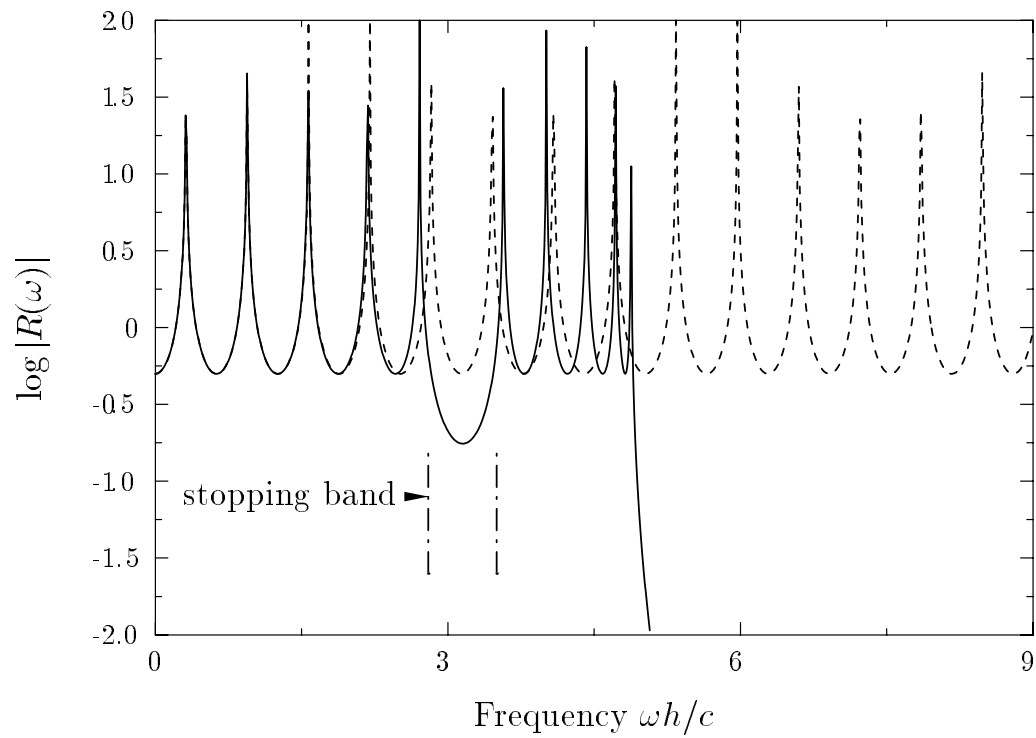


**Fig. 18:** Frequency response spectrum for Dirichlet-Fixed rod using quadratic Spectral elements

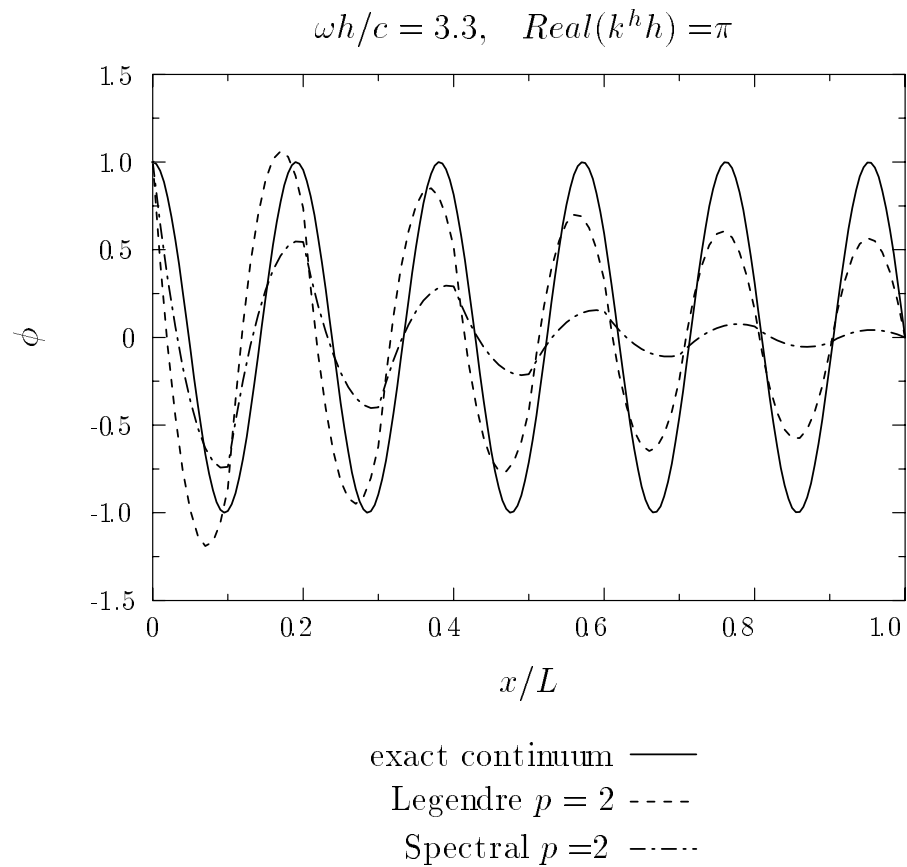


**Fig. 19:** Attenuated wave solution in the stopping band

mesh. Discrete eigenvalues  $\omega_j h/c$  are calculated from the dispersion relation (32) in which real frequency roots are sought for the given real eigenmodes  $k_j h$ . The result is a characteristic polynomial in  $\alpha_j = \omega_j h/c$  of order  $2p$ .

$$\sum_{l=0}^p c_l \alpha_j^{2l} = 0 \quad (61)$$

#### 4.2.1 Low-order elements

For linear elements with consistent mass the characteristic equation and its roots are,

$$c_0 + c_1 \alpha_j^2 = 0 \quad (62)$$

where

$$\begin{aligned} c_0(k_j h) &= 6(\cos k_j h - 1) \\ c_1(k_j h) &= (2 + \cos k_j h) \end{aligned}$$

For example, consider a mesh of two linear elements ( $p = 1, L = 2h$ ) with consistent mass and restrained ends, the number of free variables is one and the only real eigenmode for the mesh is  $k_1 h = \pi/2$ . The corresponding eigenvalue is  $w_1 h/c = \sqrt{3}$ . The exact value is  $w_1 h/c = \pi/2$ .

For a mesh of  $N = 10$  linear elements, the nine eigenvalues calculated from (62) are plotted as tick marks on the dispersion curves of Figure 1a and fall below the cut-off frequency.

#### 4.2.2 Higher-order elements

For quadratic Legendre elements, the characteristic equation and its roots are,

$$c_0 + c_1 \alpha_j^2 + c_2 \alpha_j^4 = 0 \quad (63)$$

where

$$\begin{aligned} c_0(k_j h) &= 20(1 - \cos k_j h) \\ c_1(k_j h) &= -2(13 + 2 \cos k_j h)/3 \\ c_2(k_j h) &= (3 - \cos k_j h)/12 \end{aligned}$$

$$\left(\frac{\omega_j h}{c}\right)_1^2 = \frac{-c_1 - \sqrt{c_1^2 - 4c_0c_2}}{2c_2} \quad (64)$$

$$\left(\frac{\omega_j h}{c}\right)_2^2 = \frac{-c_1 + \sqrt{c_1^2 - 4c_0c_2}}{2c_2} \quad (65)$$

For a uniform mesh with  $N = 10$  quadratic elements, the nineteen discrete frequencies calculated from (63) are plotted as tick marks on the dispersion curves in Figure 3a. The second root corresponds to the upper branch (optical branch) and is plotted with alias  $k_j h = 2\pi - k_j h$ . At the stopping band  $k_j h = \pi$ , there is a discontinuity in the frequency/wavenumber relation, where there are two possible choices for the roots. Eigenfrequencies in the range between these roots are skipped over. From numerical results, we find that the eigenfrequency occupies the lowest energy mode at this wavenumber and falls on the smaller of the two roots. The discrete eigenfrequencies fall exactly on these dispersion curves; below the cut-off frequency and outside the stopping band. These results demonstrate that the real part of the complex wavenumber Fourier analysis accurately predicts the discrete eigenfrequency spectrum for the example boundary value problem. The results of the Fourier analysis can also be used to obtain the maximum eigenfrequency (spectral radi) for p-type element discretizations, see Deville and Mund (1992).

### 4.3 Eigenmodes

It can be shown that the eigenvectors for a uniform mesh of p-version finite elements are,

$$\psi_j(x_n) = \sin(k_j x_n) = \sin(j\pi x_n/L) \quad j = 1 : pN - 1 \quad (66)$$

Comparing this result to the analytical eigenfunctions, the eigenvectors are nodally exact for all spectral orders. Figure 20 shows an example of mode  $j = 8$  for a uniform mesh of ten linear elements, while Figure 21 shows an example of mode  $j=18$  representing a wavenumber in the upper optical branch of a uniform mesh of ten quadratic elements. At the nodal points  $n$ , the amplitude  $A_1$  is exact, whereas at the intermediate points  $n \pm 1/2$  the amplitude  $A_2$  is given by the ratio  $r = A_2/A_1$  defined earlier in Figure 14. For mode  $j = 18$ , there are two aliased wave solutions, one passing through each set of points  $n$  and  $n \pm 1/2$ ,

$$\phi_n = A_1 \sin(\beta_2 n) \quad n = 0 : N \quad (67)$$

$$\phi_{n+1/2} = A_2 \sin(\beta_2(n + 1/2)) \quad n = 0 : N - 1 \quad (68)$$

where  $\beta_2 = (2\pi - \beta_{18}) = \pi/5$ , see Figure 22.

Using information obtained from the complex Fourier analysis, mode shapes for higher-order elements can be processed in order to isolate individual wave components. By superposition of these wave components, a single wave solution can be constructed with a global sinusoidal interpolation. The global sinusoidal interpolation of nodal data improves the representation of the eigenmode at inter-nodal points. For example, for mode  $j = 18$  for the quadratic finite element mesh, by applying a discrete sine transformation, see Bellanger (1989) with sample points  $\phi_m$ , i.e.

$$w_j = \frac{1}{N} \sum_{m=1}^{2N-1} \phi_m \sin\left(\frac{j m \pi}{2N}\right), \quad j = 1 : 2N - 1 \quad (69)$$

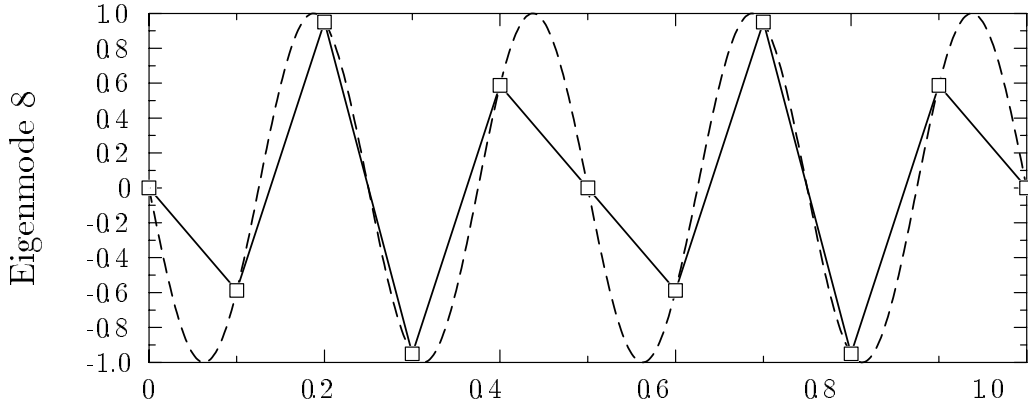


Fig. 20: Mode shape  $j = 8$  for linear finite element discretization

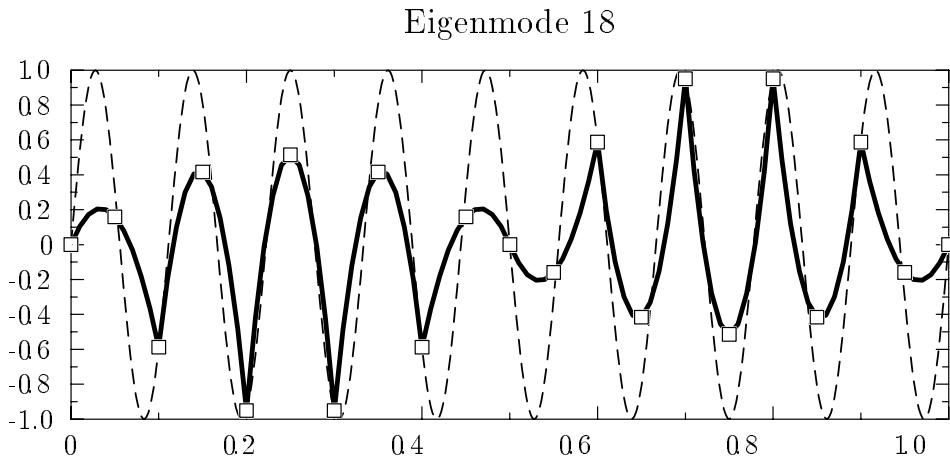


Fig. 21: Mode shape  $j = 18$  for quadratic Legendre element discretization

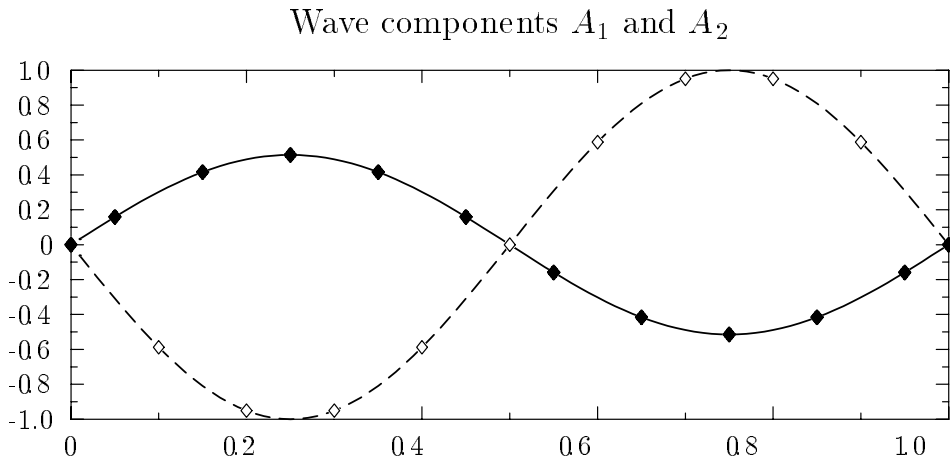
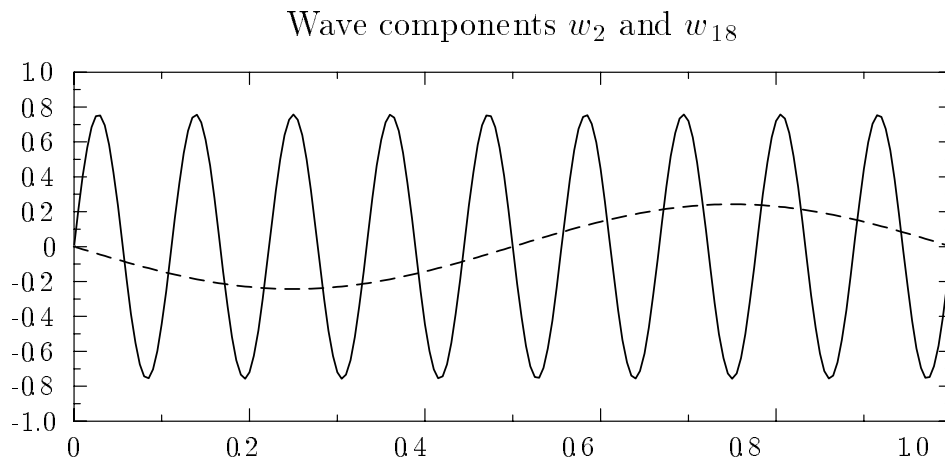
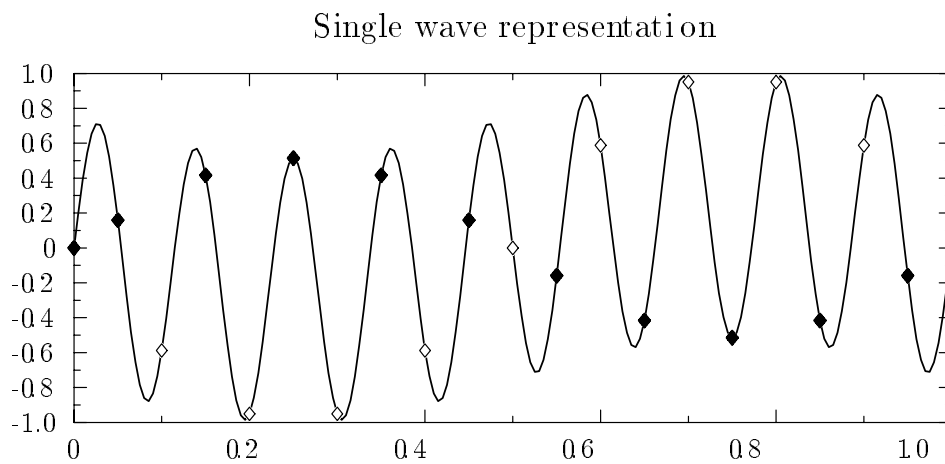


Fig. 22: Two aliased wave solutions for mode  $j = 18$ ; one passing through each set of points  $n$  and  $n \pm 1/2$ .



**Fig. 23:** Two wave components obtained from discrete sine transform of mode  $j = 18$ .



**Fig. 24:** Single wave sinusoidal interpolation for mode  $j = 18$ .

we find that the only nonzero wave amplitudes are  $w_2$  and  $w_{18}$  illustrated in Figure 23. Using the inverse sine transform,

$$\phi_m = \sum_{j=1}^{2N-1} w_j \sin\left(\frac{jm\pi}{2N}\right) = w_2 \sin\left(\frac{m\pi}{10}\right) + w_{18} \sin\left(\frac{9m\pi}{10}\right) \quad (70)$$

we then superimpose these two wave components to form the single wave constructed from the sinusoidal interpolation,

$$\phi(x) = \sum_{j=1}^{2N-1} w_j \sin\left(\frac{jx}{L}\right) \quad (71)$$

see Figure 24. Comparing this interpolated solution to the imaginary part of (51) we recognize the two wave amplitudes as  $w_2 = C_+$  and  $w_{18} = C_-$ . Although the amplitude of the sinusoidal interpolation of the eigenmode is attenuated, the post-processed eigenmode better represents the exact sinusoidal mode shape – compare Figure 21 and 24. This result demonstrates how Fourier analysis can be used as a tool to improve p-version finite element solutions to vibration problems.

## 5 Conclusions

High-order finite element discretizations have frequency bands where the solutions are harmonic decaying waves. In these so called ‘stopping’ bands, the solutions are not purely propagating (real wavenumbers) but are attenuated (complex wavenumbers). In this paper we have extended the standard dispersion analysis technique to include complex wavenumbers in order to study the dispersion and attenuation characteristics of p-type elements up to spectral order  $p = 5$ . By allowing for complex wavenumbers, a more complete characterization of the stopping bands in the frequency spectrum of finite element discretizations has been presented.

Important results of this study are that there are  $p$  stopping bands present in the dispersion curves of p-type elements; however for large spectral orders  $p$ , the first few stopping bands are very small with minimal attenuation present and are thus not of practical significance. We have also found that high-order p-type elements display increased phase accuracy compared to low-order elements, for the same number of degrees of freedom. For example, for linear elements ( $p = 1$ ), a practical limit on phase accuracy is to require at least ten elements per wavelength. For quadratic elements ( $p = 2$ ), as few as three quadratic elements per wavelength are required to obtain accurate phase. For a spectral order of ( $p = 3$ ), only two elements per wavelength are needed to maintain phase accuracy. To resolve waves with increased accuracy while maintaining only two elements per wavelength, spectral orders of ( $p \geq 4$ ) are recommended. For well resolved waves, Spectral elements using Lagrange interpolation in conjunction with Lobatto quadrature give improved convergence rates for phase error

when compared to hierarchic elements with either Legendre or Fourier basis functions. However for nondimensional frequencies extending beyond the recommended practical limits, both dispersion and amplitude attenuation errors increase the most for Spectral elements. For nondimensional frequencies in the upper branches of the frequency spectrum, Hierarchic Legendre elements exhibit improved amplitude accuracy, while Hierarchic Fourier elements exhibit both improved amplitude and phase accuracy.

A study of the closed form p-type element solution for a canonical steady-state vibration problem demonstrated the role complex wavenumbers play in the practical solution of physical boundary value problems. The existence of the cut-off frequency and stopping bands as a result of complex wavenumbers present in the finite element solution of the example problem is clearly exposed from the frequency response spectrum. The important point here is that finite element wave solutions consist of the same numerical wavenumbers found in the complex Fourier analysis except that both outgoing and incoming waves are present. In addition, we have established the direct connection between the dispersion curves (real part of the complex wavenumber characteristic relation) and the discrete eigenvalue spectrum for the example problem. In this case, all eigenmodes (wavenumbers) are real, and thus the real eigenvalues (eigenfrequencies) all fall below the cut-off frequency and outside the complex wavenumber stopping bands.

Finally, we have shown how p-type finite element solutions can be post-processed using information obtained from a complex wavenumber Fourier analysis in order to isolate component waves. By superposition of these wave components, a single wave sinusoidal interpolation can be constructed. The global sinusoidal interpolation of nodal data improves the representation of the eigenmode at inter-nodal points. This process demonstrates how results from a complex wavenumber Fourier analysis can be used as a tool to help improve p-version finite element solutions to vibration problems. The relationship between the wavenumbers predicted by complex Fourier analysis and those present in the finite element solution of boundary value problems can be studied further by post-processing the discrete finite element data with a high resolution parameter estimation technique. Wavenumbers extracted from a parameter estimation of the finite element data can then be compared to dispersion curves. In this paper, we have demonstrated that for simple boundary conditions the results will correspond exactly, however it remains to be seen what correspondence occurs for mixed boundary conditions such as the nonreflecting boundary conditions used in infinite domain problems.

Complex wavenumber dispersion analysis can also be used as a powerful tool to help design more accurate finite element approximations. The Galerkin/least-squares (GLS) modification to the standard Galerkin finite element method involves the selection of a frequency dependent parameter designed to minimize numerical dispersion over a wide range of frequencies. Presently, only the optimal GLS parameter for low-order ( $p = 1$ ) elements in one-dimension is available, see Harari and Hughes (1991a).

We have completed an analysis for the optimal selection of GLS parameters in multi-dimensions and higher-order quadratic ( $p = 2$ ) elements; the results are reported in Thompson and Pinsky (1995).

## **Acknowledgments**

This research was supported by the Office of Naval Research under contracts N00014-89-J-1951 and N00014-89K-0027. The first author was also supported in part by an Achievement Rewards for College Scientists (ARCS) scholarship. This support is gratefully acknowledged. We would also like to thank Raja Jasti and Karl Grosh for useful discussions.

## **References**

- Abboud, N.N.; Pinsky, P.M. (1992): Finite element dispersion analysis for the three-dimensional second-order scalar wave equation. *Int. J. Numer. Meth. Eng.* 35, 1183-1218
- Alvin, K.F.; Park, K.C. (1991): Frequency-window tailoring of finite element models for vibration and acoustics analysis. In: Keltie, R.F. (ed): *Structural acoustics*. vol. NCA-vol.12/AMD-vol.128, pp. 117-128. ASME
- Babuska, I.; Craig, A.; Mandel, J.; Pitkaranta, J. (1991): Efficient preconditioning for the p-version finite element method in two-dimensions. *SIAM J. Num. Anal.* 28, 624-661
- Babuska, I.; Suri, M. (1990): The p- and h-p versions of the finite element method, an overview. *Comp. Meth. in Appl. Mech. Eng.* 80, 5-26
- Barragy, E.; Carey, G.F. (1991): Preconditioners for high degree elements. *Comp. Meth. in Appl. Mech. Eng.* 93, 97-110
- Bayliss, A.; Goldstein, C.I.; Turkel, E. (1985): On accuracy conditions for the numerical computation of waves. *J. Comp. Phys.* 59, 396-404
- Bellanger, M. (1989): *Digital Processing of Signals*. John Wiley and Sons
- Belytschko, T.B.; Mindle, W.L. (1980): Flexural wave propagation behaviour of lumped mass approximations. *Computers and Structures.* 12, 805-812
- Belytschko, T.B.; Mullen, R. (1978): On dispersive properties of finite element solutions. In: Miklowitz, J. (ed): *Modern problems in elastic wave propagation*, pp. 67-82
- Brillouin, L. (1953): *Wave propagation in periodic structures*. Dover
- Canuto, C.; Hussaini, M.Y.; Quarteroni, A.; Zang, T.A. (1988): *Spectral methods in fluid dynamics*. Springer-Verlag

Churchill,R.V.; Brown,J.W.; Verhey,R.F. (1976): Complex variables and applications. McGraw-Hill

Deville,M.O.; Mund,E.H. (1992): Fourier analysis of finite element preconditioned collocation schemes. SIAM J. Sci. Stat. Comp. 13,596-610

Fischer,P.F.; Patera,A.T. (1991): Parallel spectral element methods for the incompressible Navier-Stokes equations. In: Supercomputing, pp. 71-143. ASME

Friberg,O.; Moller,P. (1987): An adaptive procedure for eigenvalue problems using the hierarchical finite element method. Int. J. Num. Meth. Ing. 24, 319-335

Grosh,K.; Pinsky,P.M. (1996): Design of Galerkin Generalized Least Squares Methods for Timoshenko Beams. Comp. Meth. in Appl. Mech. Eng., 132, pp. 1-16.

Harari,I.; Hughes,T.J.R. (1991a): Computational methods for problems of acoustics with particular reference to exterior domains. Tech. Report SUDAM No. 91-1, Stanford University

Harari,I.; Hughes,T.J.R. (1991b): Finite element methods for the Helmholtz equation in an exterior domain: Model problems. Comp. Meth. in Appl. Mech. Eng. 87, 59-96.

Hughes,T.J.R.; Franca,L.P.; Hulbert,G.M. (1989): A new finite element formulation for computational fluid dynamics: VIII. The galerkin least squares method for advective-diffusive equations. Comp. Meth. in Appl. Mech. Eng. 73, 173-189

Jasti,R. (1992): Mixed shell finite elements with applications in structural acoustics. Ph.D. Thesis, Stanford University

Maday,Y.; Patera,A.T. (1989): Spectral element methods for the incompressible Navier-Stokes equations. In: Noor,A.K.; Oden,J.T. (ed): State-of-the-art surveys on computational mechanics. PP. 71-143, ASME

Mindle,W.L.; Belytschko,T. (1983): A study of shear factors in reduced-selective integration Mindlin beam elements. Computers and Structures. 17, 339-344

Park,K.C.; Flaggs,D.L. (1984): A Fourier analysis of spurious mechanisms and locking in the finite element method. Comp. Meth. in Appl. Mech. Eng. 46, 65-81

Park,K.C.; Flaggs,D.L. (1985): A symbolic Fourier synthesis of a one-point integrated quadrilateral plate element. Comp. Meth. in Appl. Mech. Eng. 48, 805-812

Patera,A.T. (1984): A spectral element method for fluid dynamics: Laminar flow in a channel expansion. J. Comp. Phys. 54, 468-488

Shakib,F.; Hughes,T.J.R. (1991): A new finite element formulation for computational fluid dynamics: IX. Fourier analysis of space-time Galerkin/least-squares algorithms. *Comp. Meth. in Appl. Mech. Eng.* 87, 35-58

Silva,M.A.G. (1991): Study of pass and stop bands of some periodic composites. *Acustica.* 75, 62-68

Szabo,B.; Babuska I. (1991): *Finite element analysis.* John Wiley and Sons

Thompson,L.L.; Pinsky,P.M. (1995): A Galerkin/least-squares finite element method for the two-dimensional helmholtz equation. *Int. J. Num. Meth. Eng.*, Vol. 38, pp. 371-397.

Underwood,P. (1974): Accuracy of finite difference representations for the transient response analysis of shells. *Earthquake Eng. and Struc. Dynam.* 2, 219-233

Voight,R.G.; Gottlieb,D; Hussaini,M.Y. (1984): *Spectral methods for partial differential equations.* SIAM

Wolfram,S. (1991): *Mathematica.* Addison-Wesley